Progress in Earth and Planetary Science
a SpringerOpen Journal

RESEARCH Open Access

Typhoon-induced sea surface cooling during the 2011 and 2012 typhoon seasons: observational evidence and numerical investigations of the sea surface cooling effect using typhoon simulations

Akiyoshi Wada[1*], Tomohiro Uehara[2] and Shiro Ishizaki[2]

Abstract

Understanding oceanic responses to typhoons and the impacts those responses have on the typhoons themselves is important so that typhoon predictions performed using numerical models and typhoon forecasts can be improved. However, *in situ* oceanic observations underneath typhoons are still limited. To gain a deep understanding of the oceanic response and estimate the magnitude of its impact, three profiling floats were deployed in the western North Pacific during the 2011 and 2012 typhoon seasons. The daily observations showed that the sea surface cooled by more than 2°C in typhoons Ma-on and Muifa in 2011, and typhoons Bolaven and Parapiroon in 2012. The response was different at different float locations relative to the typhoon center, that is, the response within 100 km of the typhoon center was different to the response more than 100 km from the center on the right- or left-hand sides of the typhoon track, even though the response was affected by pre-existing oceanic conditions, precipitation, and the typhoon intensity. The salinity and temperature profiles were also considerably different before, during, and after the passage of a typhoon. To determine the impacts of typhoon-induced sea surface cooling on typhoon predictions, the impacts of the four typhoons were numerically evaluated using an atmosphere-wave-ocean coupled model. The coupled model simulated sea surface cooling and the resultant increases in the central pressures caused by the passages of the typhoons reasonably well. When axisymmetrically simulated, the mean sea surface cooling beneath a typhoon decreased the latent heat fluxes by 24% to 47%. A larger cooling effect gave a larger decrease in the latent heat flux only during the intensification phase. The decrease in the latent heat flux affected the inner core structure, particularly in the inflow boundary layer and around the eyewall. The cooling effect significantly affected the track simulation only for Typhoon Muifa, which had the weakest zonal steering flow of the four typhoons. These results suggest that making more frequent typhoon observations using profiling floats, further developing oceanic analysis techniques, and improving our understanding of typhoon-ocean interactions are required to produce more accurate typhoon predictions.

Keywords: Typhoon; Profiling float; Sea surface cooling; Latent heat flux; Atmosphere-wave-ocean coupled model

Background

Advances in observational technologies, data assimilation systems, and numerical modeling have made it possible to predict tropical cyclones (TCs) more precisely than was previously the case. Little progress has been made, however, in predicting TC intensities, despite notable improvements in TC track predictions in recent decades. In particular, the dynamics and thermodynamics associated with rapid intensification are not well understood, and simulations using numerical prediction systems sometimes overestimate or underestimate TC intensities and intensification rates. It has previously been stated that understanding interactions between TCs and the ocean is crucial to decreasing the extent of the overestimations that are currently made of TC intensities (Bender et al. 1993; Shade and Emanuel 1999) and intensification rates (Wada 2009).

* Correspondence: awada@mri-jma.go.jp
[1]Meteorological Research Institute, Japan Meteorological Agency, 1-1 Nagamine, Tsukuba, Ibaraki 305-0052, Japan
Full list of author information is available at the end of the article

A TC will induce sea surface cooling in its wake (Price 1981; Wada 2002; Walker et al. 2005; D'Asaro et al. 2011; Pun et al. 2011; Jeong et al. 2013). This and other oceanic responses to a TC have been the subjects of numerous studies (e.g., Shay 2010), and highly complex physical processes associated with typhoon-ocean interactions have recently been investigated in a large typhoon-ocean field experiment ('Impact of Typhoons on the Ocean in the Pacific') (D'Asaro et al. 2011; Pun et al. 2011). In the western North Pacific, TCs with maximum sustained wind speeds exceeding approximately 33 m s^{-1} are called 'typhoons,' and the Japanese term *taifu* means a TC with a maximum sustained wind speed exceeding approximately 17 m s^{-1}. It has previously been reported that TC-induced sea surface cooling is mainly caused by Ekman upwelling and vertical turbulent mixing (Price 1981; Wada et al. 2009a; Sanford et al. 2011). The rate of entrainment at the base of the mixed layer caused by the passage of a TC is primarily determined by different horizontal current speeds at different depths across the base (Price 1981; Sanford et al. 2007). Wada et al. (2010) suggested that vertical turbulent mixing caused by breaking surface waves caused by a TC also plays an important role in sea surface cooling. The effect of vertical turbulent mixing on TC-induced sea surface cooling depends very much on the speed at which the TC moves (Wada et al. 2009a; Lin 2012).

Sea surface cooling induced by a TC is also affected by pre-existing oceanic conditions such as the depth of the mixed layer and the temperature gradient within the underlying thermocline (Price 1981; Wada 2002; Moon and Kwon 2012). In particular, the passage of a TC over a warm eddy will decrease the magnitude of the sea surface cooling that occurs (Wu et al. 2007; Wada et al. 2010). The presence of a warm eddy beneath a TC will, therefore, enable the TC to become intensified more rapidly than would be the case otherwise, because the air-sea sensible and latent heat fluxes increase rapidly (Lin et al. 2005, 2008, 2009; Wada and Usui 2007; Shay 2010). It can be seen that the mechanisms involved in TC-induced sea surface cooling are complex and depend on various factors, such as the TC intensity, translation speed, and size, and on pre-existing oceanic conditions such as the depth of the mixed layer and the temperature gradient within the underlying seasonal thermocline. *In situ* observations underneath a TC are, therefore, needed to allow the mechanisms involved in TC-induced sea surface cooling to be determined.

Decreased enthalpy (sensible and latent heat) fluxes underneath a TC are caused by TC-induced sea surface cooling. Cione and Uhlhorn (2003) found that sea surface cooling of approximately 1°C within the inner core of a TC can effectively alter the maximum total enthalpy flux by 40% or more. A lower translation speed will cause a much higher enthalpy flux to be required to maintain the intensity of an intense TC (Lin et al. 2009). However, the dependence of the decrease in enthalpy (particularly latent heat) flux within the inner core on TC-induced sea surface cooling has not yet been effectively determined.

The atmospheric response to TC-induced sea surface cooling and the impact such a response has on an idealized TC-like vortex has been investigated using atmosphere-ocean coupled models (Chang and Anthes 1979; Zhu et al. 2004; Wu et al. 2005; Bender et al. 2007; Wada 2009), and an atmosphere-wave-ocean coupled model has recently been developed to numerically simulate TCs (Chen et al. 2007, 2013; Wada et al. 2010, 2013; Warner et al. 2010). It has been shown in numerical experiments that TC-induced sea surface cooling leads to the suppression of the intensity of an idealized TC-like vortex, resulting in decreased latent heat fluxes within the inner core of the vortex and increased inner-core asymmetries (Zhu et al. 2004; Wu et al. 2005). However, the effects of interactions between the atmospheric and oceanic environments on TC evolution were not examined using these idealized numerical experiments. Numerical simulations of TCs using atmosphere-wave-ocean models have, so far, provided only preliminary results. The degree to which TC-induced sea surface cooling and the associated decreased latent heat flux affects the intensity of a TC in realistic atmospheric and oceanic environments is still uncertain, as is how the sea surface cooling and decreased latent heat flux affect the inner core structure of a TC.

This study aims to present the following: first, to determine the oceanic response to the passage of a typhoon using daily *in situ* observations made by profiling floats deployed in the western North Pacific Ocean and second, to quantitatively evaluate the effect of the oceanic response on the typhoon predictions produced using an atmosphere-wave-ocean coupled model, especially when the observed extent of sea surface cooling exceeded 2°C. The observations made by the profiling floats will be outlined in the next subsection.

Observations made by profiling floats during the 2011 and 2012 typhoon seasons

Profiling floats are autonomous instruments that drift with ocean currents while measuring the water temperature, salinity (as conductivity), and pressure (i.e., depth) as they ascend through the water column. Three profiling floats, each with an Iridium communication system, were deployed around 20°N (World Meteorological Organization (WMO) number 5901989, identification number (ID) 6399), 22°N (WMO number 5901988, ID 7560), and 24°N (WMO number 2901670, ID 6429) along the 137°E meridian by the R/V Keifu Maru, which is operated by the Japan Meteorological Agency (JMA), on 22 and 23 June 2011 (Figure 1). The profiling floats were used to monitor rapid

variations in the water temperature and salinity in the upper ocean caused by the passage of typhoons during the 2011 and 2012 seasons. A bidirectional telecommunication system was used, and the three profiling floats recorded vertical profiles of the water temperature and salinity between approximately 5- and 500-m deep every day during the typhoon season (June to October) and between approximately 5- and 2,000-m deep every 10 days outside the typhoon season.

In this study, TCs with maximum wind speeds exceeding approximately 17 m s^{-1} (called *taifu* in Japanese, as mentioned above) are categorized as typhoons. Each typhoon is referred to by its number, Tyynn, where yy are the last two digits of the year and nn is the sequential number for the typhoon in that typhoon season. Five typhoons, Ma-on (T1106), Muifa (T1109), Talas (T1112), Kulap (T1114), and Roke (T1115), passed over the area monitored by the floats (around 17°N to 27°N and 130°E to 140°E) during the 2011 typhoon season, and three typhoons, Bolaven (T1215), Sanba (T1216), and Prapiroon (T1221), passed over the area monitored by the floats (around 20°N to 27°N and 125°E to 135°E) during the 2012 typhoon season (Figure 1).

The names and numbers of these eight typhoons, the analysis period for each typhoon, and the maximum amount of sea surface cooling that was observed by the three profiling floats during each analysis period are shown in Table 1. The analysis period is the period during which the typhoon passed over the area monitored by the profiling floats (Figure 1), and the maximum amount of sea surface cooling, which ranged from 0.8°C to 4.3°C (Table 1), was defined as the difference between the maximum and minimum water temperature at a depth of 5 m during each analysis period.

Regarding the relationship between the maximum amount of sea surface cooling and the TC, it has been suggested that TC-induced sea surface cooling of more than 2.5°C will not cause the intensification of a TC because this degree of cooling should be sufficient to shut down the entire energy production process of the TC (Emanuel 1999; Emanuel et al. 2004; Lin et al. 2008). The amount of cooling that occurred during typhoons T1106, T1109, and T1221 exceeded this threshold (Table 1), and the sea surface was cooled by 2°C, which is close to the threshold, during typhoon T1215. We will later assess the changes in water temperature and salinity profiles during the passage of four typhoons (T1106, T1109, T1215, and T1221) and perform numerical simulations of the typhoons using an atmosphere-wave-ocean coupled model.

The three profiling floats drifted westward in the 2 years wherein the observations were made (Figure 1), mainly following the wind-driven North Equatorial Current (Qiu and Chen 2010), and they sometimes became trapped in mesoscale eddies. The areas in which the observations were made in the 2011 and 2012 seasons were, therefore, different (Figure 1). However, the

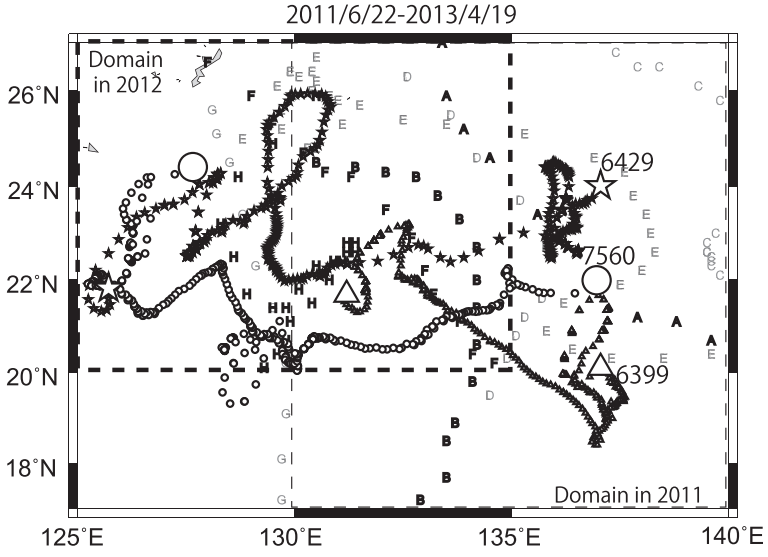

Figure 1 Trajectories of the three profiling floats from 22 June 2011 to 19 April 2013. All of the profiling floats were deployed along the 137°E meridian on 22 and 23 June 2011. The first symbols accompanying the float IDs (stars for 6429, circles for 7560, and triangles for 6399) indicate the locations where the floats were initially deployed, and the second symbols indicate the locations of the floats on 19 April 2013. The letters in bold indicate the central positions of the typhoons listed in Table 1 (A, T1106; B, T1109; C, T1112, D, T1114; E, T1115; F, T1215; G, T1216; and H, T1221) every 6 h. The bold characters show when a profiling float was within 300 km of a typhoon track. The thin dashed box indicates the domain wherein the three profiling floats were monitored in 2011, and the thick dashed box indicates the domain wherein the three profiling floats were monitored in 2012.

Table 1 Typhoons and the maximum sea surface cooling observed during the typhoons by the profiling floats

Name	Number	Analysis period	Maximum sea surface cooling (°C) (float ID)
Ma-on	T1106	15 to 18 July 2011	4.3 (6429)
Muifa	T1109	31 July to 3 August 2011	3.5 (7560)
Talas	T1112	24 to 30 August 2011	1.1 (6429)
Kulap	T1114	6 to 8 September 2011	1.0 (6399)
Roke	T1115	10 to 19 September 2011	0.8 (7560)
Bolaven	T1215	23 to 26 August 2012	2.0 (6399)
Sanba	T1216	14 to 16 September 2012	0.8 (6429)
Prapiroon	T1221	12 to 17 October 2012	3.3 (6399)

horizontal distributions of weekly sea level height anomalies indicated that the locations of warm eddies and cold wakes changed little over the time taken for a typhoon to pass (a week), although the amplitudes of the cold wakes became stronger after a typhoon had passed over than before it had arrived (Figure 2). Weekly sea level height anomaly observations made by a satellite-borne altimeter were obtained from the Archiving, Validation and Interpretation of Satellite Oceanographic data (AVISO) website (http://www.aviso.oceanobs.com/). On the basis of the results shown in Figure 2, we assumed that weekly mesoscale oceanic variations caused by planetary Rossby waves were negligible compared with variations caused by the response of the ocean to a typhoon. The cold wake area, with a negative sea surface height anomaly, corresponded with the area of relatively low sea surface temperatures (sea surface cooling) that was formed after the passage of each typhoon (Figure 3). The horizontal sea surface temperature distributions were obtained from the daily dataset produced by the Tropical Rainfall Measuring Mission (TRMM) microwave imager (TMI), and the Aqua/Advanced Microwave Scanning Radiometer for Earth observing system (AMSRE) satellite radiometers, which have a horizontal resolution of 0.25° (http://www.ssmi.com/). A remarkable amount of sea surface cooling occurred along the path of each typhoon after it had passed, except for T1221 (Figure 3i,j,k,l).

Figure 4 shows the trajectories of the three profiling floats and the best tracks (from the Regional Specialized Meteorological Center-Tokyo (RSMC-Tokyo) best-track data) for T1106, T1109, T1215, and T1221, along with three-hourly accumulated precipitation measurements collected during the analysis period (Table 1) for each typhoon (when the typhoon entered the domain shown in Figure 4). The three-hourly global precipitation estimates at a resolution of 0.25° latitude and 0.25° longitude produced by the US National Oceanic and Atmospheric Administration (NOAA) Climate Prediction Center morphing method (Joyce et al. 2004) were used to determine the total precipitation distribution during each analysis period. The horizontal total precipitation distribution indicated that the total precipitation was higher in T1221 than in T1106, T1109, and T1215, and this was caused by the relatively slow and irregular track followed by T1221.

Methods

Profiling floats

Vertical profiles of the water temperature and salinity were obtained from three profiling floats during their ascents. Real-time quality control was performed before the data were made available on the Japan Argo Real Time Data Base (http://argo.kishou.go.jp/index.html), which is operated by the Japan Meteorological Agency, from which the data used in this study were taken. Daily water temperature and salinity observations made by the three profiling floats were interpolated from the subsurface (at a depth of nearly 5 m) to a depth of 200 m using the method developed by Akima (1970). The temperature and salinity between the surface and a depth of 5 m were assumed to be constant, because no surface observations were made by the profiling floats. The maximum sea surface cooling values (Table 1) were calculated from the water temperatures observed at a depth of 5 m during each analysis period. This method is valid when surface wind speeds are higher than approximately 7 m s^{-1} (Soloviev and Lukas 2006; Kawai and Wada 2007). Soloviev and Lukas (2006) showed that the water was well mixed (in terms of temperature) between the subsurface and a depth of 5 m under relatively strong winds (approximately 7 m s^{-1}) in the Pacific warm pool during the Coupled Ocean-Atmosphere Response Experiment.

The mixed layer was defined as the water down to a depth at which the density was 0.25 g m^{-3} higher than the density at the surface, whereas the isothermal layer was defined as the water down to a depth at which the temperature was 0.5°C different from the temperature at the surface.

Model

The nonhydrostatic model (NHM) that was used in this study was developed jointly by the JMA Numerical Prediction Division and the Meteorological Research Institute (MRI). The model is a regional mesoscale atmospheric model that includes physical processes (see Table 2) (such as clouds, which are described using an explicit three-ice bulk microphysics scheme that is based on the work published by Lin et al. (1983)), an assumed resistance law for the air-sea momentum and for enthalpy fluxes in the atmospheric surface boundary layer, exchange coefficients for the air-sea momentum and for enthalpy transfers over the sea (based on bulk formulae (Kondo 1975) or when the ocean-wave model is coupled (Wada et al. 2010), based on the roughness lengths proposed by Taylor and

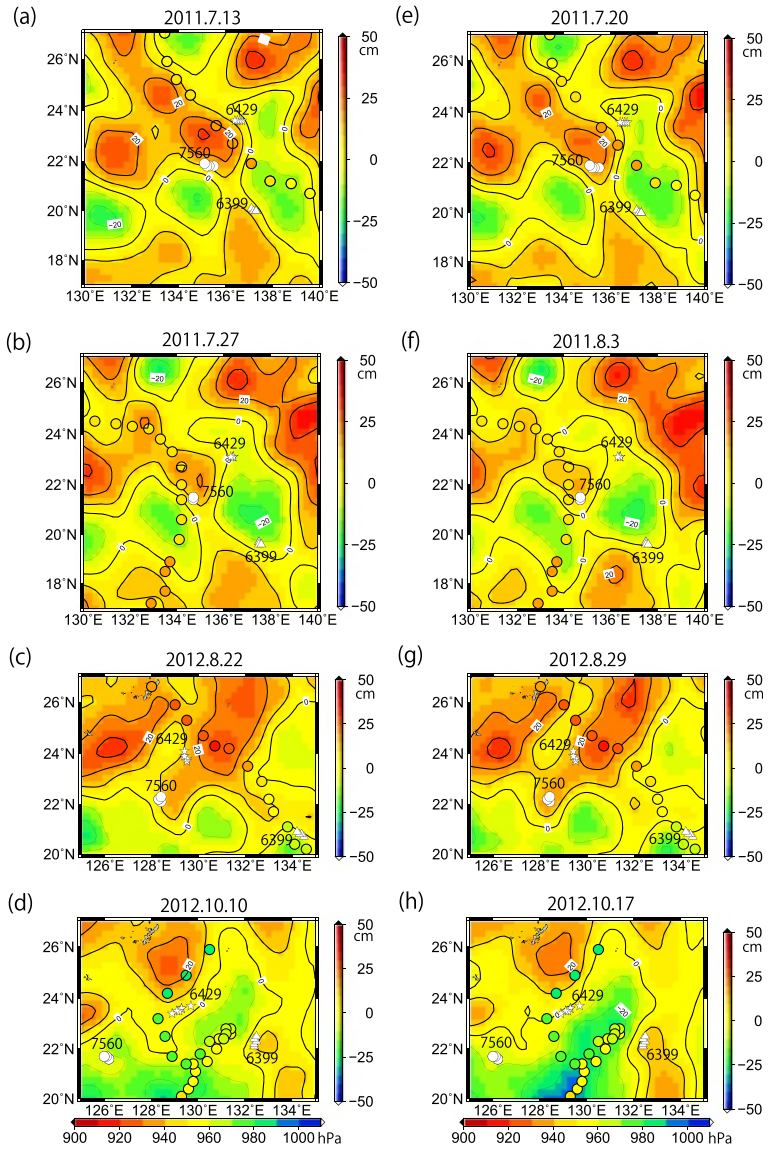

Figure 2 Horizontal distributions of the AVISO weekly sea surface height anomaly. Horizontal distributions of the AVISO weekly sea surface height anomaly (cm) (http://www.aviso.oceanobs.com/) on **(a)** 13 July 2011, **(b)** 27 July 2011, **(c)** 22 August 2012, and **(d)** 10 October 2012 before the passage of a typhoon and on **(e)** 20 July 2011, **(f)** 3 August 2011, **(g)** 29 August 2012, and **(h)** 17 October 2012 after the passage of the typhoons. The colors within the circles indicate the central pressure of the typhoon at each position along the RSMC-Tokyo best track. The open stars, circles, and triangles show the positions of the profiling floats, as in Figure 1, except during each analysis period.

Yelland (2001)), a turbulent closure model in the atmospheric boundary layer (based on the work of Klemp and Wilhelmson (1978) and Deardorff (1980)), and an atmospheric radiation scheme (based on the work of Sugi et al. (1990)). The NHM used was an older version of the current nonhydrostatic mesoscale model (Saito 2012), and it was coupled with both a multilayer ocean model and a third-generation ocean-wave model (Wada et al. 2010). No cumulus parameterization was used.

The JMA third-generation ocean-wave model was coupled with the NHM to estimate changes in the surface roughness lengths, drag coefficients, and enthalpy coefficients. The wave spectrum in the third-generation ocean-wave model had 900 components, each associated with one of 25 frequencies and one of 36 directions. The frequency of the wave spectrum was divided logarithmically from 0.0375 to 0.3000 Hz. The ocean was assumed to be motionless at the initial time. Wada et al. (2010) described the wave-ocean coupling procedure in detail.

The multilayer ocean model used a decreased gravity approximation and a hydrostatic approximation, and it was assumed that the water was a Boussinesq fluid. The

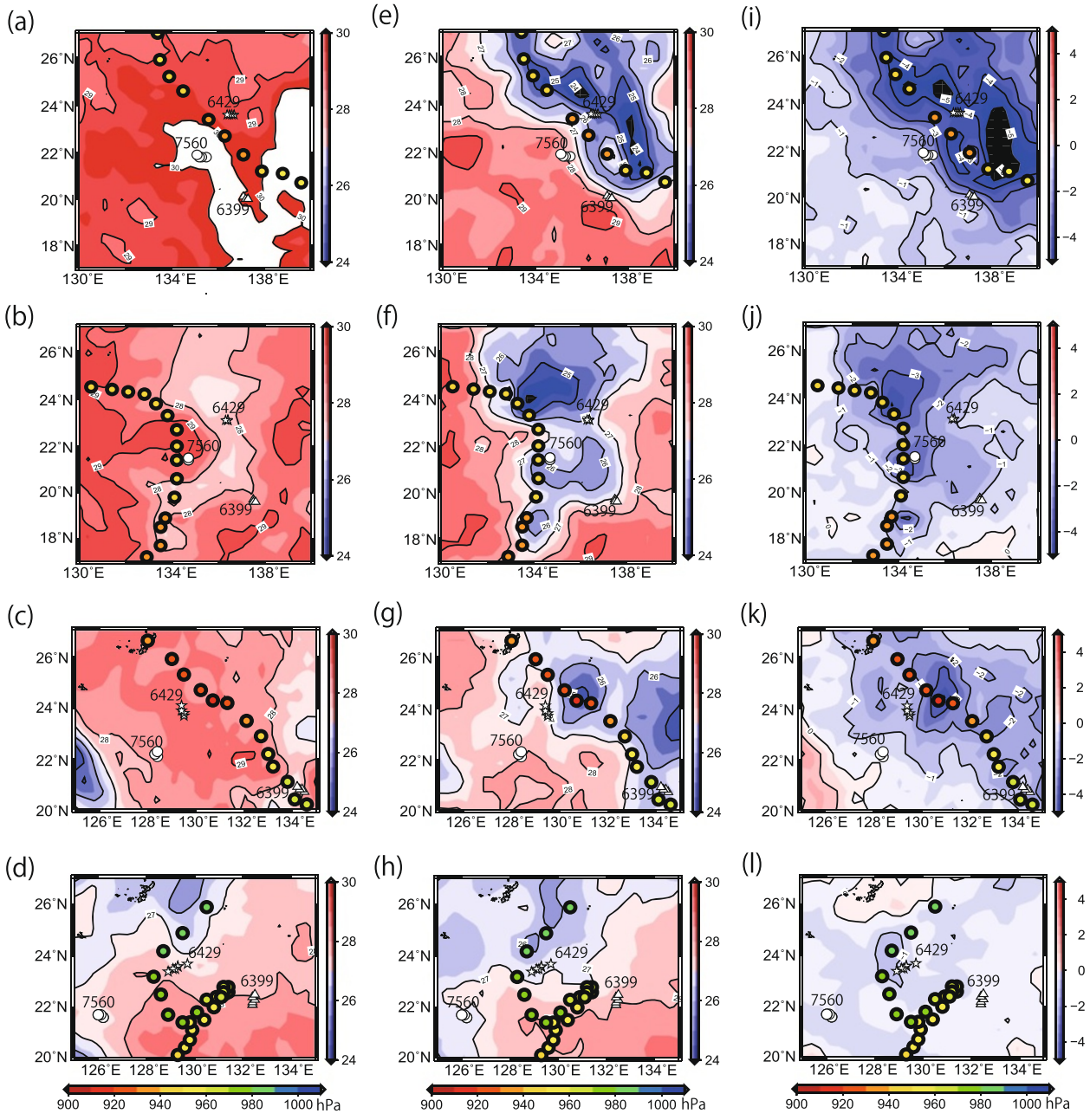

Figure 3 Horizontal distributions of TRMM/TMI sea surface temperatures. Horizontal distributions of TRMM/TMI sea surface temperatures (°C) on **(a)** 15 July 2011, **(b)** 31 July 2011, **(c)** 23 August 2012, and **(d)** 12 October 2012 before the passage of a typhoon and on **(e)** 18 July 2011, **(f)** 3 August 2011, **(g)** 26 August 2012, and **(h)** 17 October 2012 after the passage of the typhoons. **(i** to **l)** Differences in the TRMM/TMI sea surface temperature between before and after the passage of the typhoon (before subtracted from after). The colors within the circles indicate the central pressure of the typhoon at each position along the RSMC-Tokyo best track. The open stars, circles, and triangles show the positions of the profiling floats, as in Figure 1, except during each analysis period.

model had three layers and four levels. The uppermost layer was the mixed layer, where the density was vertically uniform. The middle layer was the seasonal thermocline, where the vertical temperature gradient was greatest. The bottom layer was assumed to be undisturbed by entrainment. The four levels were the sea surface, the mixed layer base, the thermocline base, and the sea bottom. The degree of entrainment was calculated using the multi-limit entrainment formula proposed by Deardorff (1983) and modified by Wada et al. (2009a). The model calculated the water temperature and salinity at the surface and at the base of the mixed

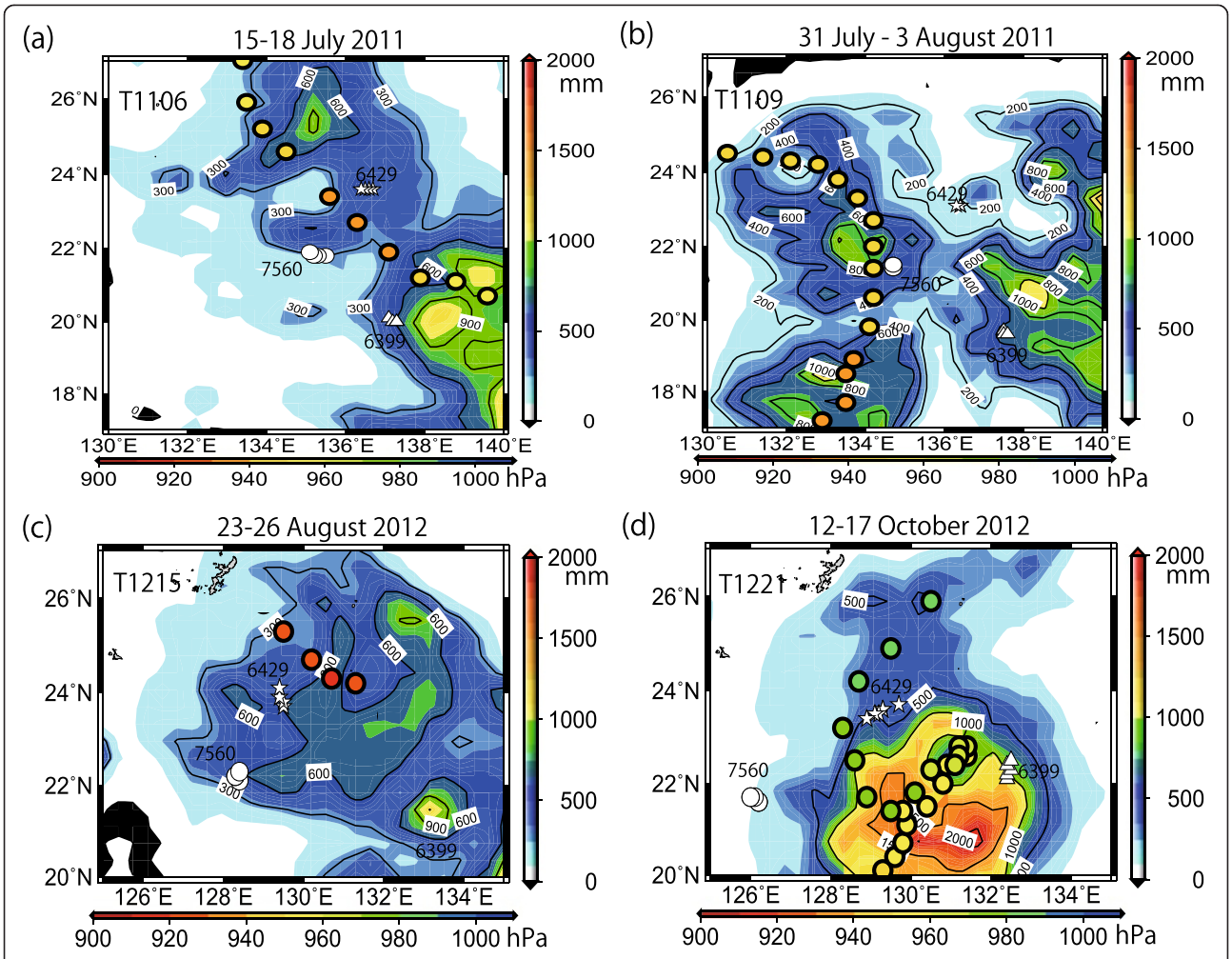

Figure 4 Horizontal distributions of three-hourly accumulated precipitation and the RSMC-Tokyo best track. Horizontal distributions of three-hourly accumulated precipitation (color shading) and the RSMC-Tokyo best track (filled circles) during the periods **(a)** 15 to 18 July 2011 for T1106, **(b)** 31 July to 3 August 2011 for T1109, **(c)** 23 to 26 August 2012 for T1215, and **(d)** 12 to 17 October 2012 for T1221. The colors within the circles indicate the central pressure of the typhoon at each position along the RSMC-Tokyo best track. The open stars, circles, and triangles show the positions of the profiling floats, as in Figure 1, except during each analysis period.

layer, and the thickness of each layer and the two-dimensional flows in the layers. The model could simulate near-inertial currents behind a TC reasonably well (Wada 2002).

The atmosphere-ocean coupling procedure is described next. Short- and long-wavelength radiation, sensible and latent heat fluxes, wind stresses, and precipitation were calculated by the atmospheric model and supplied to the ocean model at every time step in the ocean model. Land and sea distributions, extracted from the Global TOPOgraphic 30 digital elevation data produced by the US Geological Survey, were provided by the atmosphere model to the ocean model only at the initial time, to ensure that the land and sea distributions in the atmosphere and ocean models matched. The topography of the ocean bottom at 5′ latitude and longitude intervals was used in the ocean model, and these data were taken from the Earth Topography Digital Dataset 5 provided by the NOAA National Geophysical Data Center. The sea surface temperature calculated by the ocean model was provided to the atmospheric model at every time step in the ocean model.

Experimental design

The experimental design used in the numerical simulations of T1106, T1109, T1215, and T1221 are summarized in Table 2. The horizontal resolution of each typhoon simulation performed by the NHM was applied to the ocean-wave model and the multilayer ocean model. The vertical coordinates used in all of the NHM and coupled model experiments had 40 vertical levels, with different intervals ranging from 40 m for the lowermost (near-surface) layer to 1,180 m for the uppermost layer. The time

step used in the ocean model was six times the time step used in the atmosphere model, and the time step used in all of the ocean-wave model experiments was 10 min.

The initial oceanic conditions were derived from the MRI Ocean Variational Estimation (MOVE) system (Usui et al. 2006). The MOVE system directly assimilates sea level height anomalies observed by a satellite-borne altimeter (http://www.aviso.oceanobs.com/). The initial depth of the oceanic mixed layer was determined from oceanic reanalysis data by defining the mixed layer as reaching a depth at which the density was no more than 0.25 kg m^{-3} higher than the density at the surface and having a maximum depth of 200 m. The base of the thermocline was limited to 600 m, whereas the water depth was limited to 2,000 m. The integration time was relatively short, so open oceanic boundaries were used in a series of numerical simulations.

The initial atmospheric conditions and the boundary conditions were derived from six-hourly global objective analysis data provided by the JMA, with a grid spacing of 20 km. Lateral boundary conditions were provided to the computational domain every 6 h, and an appropriate domain width was set for each typhoon simulation (see Table 2). The experimental design used for the numerical simulations of T1106, T1109, T1215, and T1221, and the physical processes used in the NHM are shown in Table 2. The experimental design used for T1221L was the same as the design used for T1221H, except for the horizontal resolution of the MOVE data, which was 0.5° latitude and longitude (calculated using the North Pacific version of MOVE) for T1221L and 0.1° latitude and longitude (calculated using the western North Pacific version of MOVE) for T1221H (Usui et al. 2006).

Results and discussion

Observational evidence for the oceanic response to typhoons

In situ observations made by autonomous oceanic profiling floats have been used to investigate the oceanic response to a typhoon in previous studies. Wada et al. (2009b) found that vertical water temperature profiles obtained at 10-day intervals were clearly affected by the passage of a typhoon and that the change was dependent on the position of the profiling float relative to the typhoon track. Baranowski et al. (2011) found that the passage of two consecutive typhoons, Hagupit and Jangmi, in 2008, caused changes in the oceanic mixed layer. The *in situ* observations that showed these changes were made by an autonomous oceanic profiling float operating on a cycle with a period of approximately 1 day, and the authors showed that more frequent profiling (at least once a day) is required to allow variations in the water temperature and salinity in the upper ocean caused by the passage of a TC to be studied.

Two essential processes must be taken into account when assessing the oceanic response to a typhoon. First, vertical turbulent mixing occurs beneath a typhoon. In the Northern Hemisphere, this entrainment occurs more strongly on the right-hand side of the typhoon track (relative to the direction the typhoon moves), where the shear induced by near-inertial currents is stronger (Price 1981; Nam et al. 2012). Second, upwelling occurs behind a typhoon because of the cyclonic circulation of the surface winds (Price 1981; Wada 2002). When the translation speed of a typhoon is lower than the phase speed of the first baroclinic mode, this upwelling plays an essential role in causing sea surface cooling because a cold wake is formed behind the typhoon (Shay et al. 1998).

In this study, the variations in the water temperature and salinity in the upper ocean were studied using *in situ* daily observations made by three profiling floats. In particular, we will assess how the upper ocean responses vary according to the position of the float relative to the typhoon center and track. The evolutions of the water temperature and salinity profiles were examined in the vicinity of the typhoon (less than 100 km from the center) and more than 100 km from the center of the typhoon track on the right- or left-hand side (relative to the direction the typhoon moved). The following profiling floats and typhoon cases were selected: profiling floats 7560 and 6399 were located in the vicinity of the tracks of T1109 and T1215, respectively; profiling floats 6429 and 6399 were located more than 100 km from the nearest track on the right-hand side of the tracks of typhoons T1106 and T1221, respectively; and profiling floats 7560 and 6429 were located more than 100 km from the nearest track on the left-hand side of the tracks of typhoons T1106 and T1215, respectively (Figures 2, 3, and 4).

Figures 5, 6 and 7 show the vertical water temperature and salinity profiles that were found by the profiling floats within 100 km of the typhoon centers (Figure 5) and more than 100 km from the typhoon centers on the right-hand (Figure 6) and left-hand (Figure 7) sides of the tracks. The vertical water temperature and salinity profiles for T1109 (float 7560) and T1215 (float 6399) (Figure 5) showed that the water in the vicinity of each typhoon center was warm and that the salinity in the mixed layer was low and uniform before the passage of T1109 on 29 July 2011 and the passage of T1215 on 21 August 2012. Both the mixed and isothermal layers became deeper during the passage of both typhoons, and the water temperature abruptly decreased and the salinity abruptly increased in the mixed layer on 2 August 2011 for T1109 and 23 August 2012 for T1215. The isothermal layer was deeper than the mixed layer in both typhoons. The difference between the isothermal and mixed layer depths was caused by the upwelling of saline water in the seasonal thermocline. The seasonal thermocline became steeper during the passage of each typhoon

Table 2 Specifications of the coupled model and the experimental design for the simulations

	T1106	T1109	T1215	T1221L(H)
Horizontal resolution	2 km	2 km	2 km	3 km
Horizontal grid number	1,391 × 1,201	1,101 × 1,101	1,291 × 1,021	701 × 701
Vertical grid number	40			
Top height	22,801 m			
Time step (atmosphere model)	6 s	6 s	6 s	8 s
Initial time	2011/7/13/0000UTC	2011/7/30/0000UTC	2012/8/21/0000UTC	2012/10/8/0000UTC
Integration time	144 h	84 h	96 h	168 h
Lateral boundary relaxation sponge layers	70	100	60	15
Oceanic initial condition	MOVE 0.1°	MOVE 0.5°	MOVE 0.1°	MOVE 0.5° (0.1°)
Surface roughness length	Kondo (1975) [uncoupled model]/Taylor and Yelland (2001) [coupled model]			
Surface boundary layer	Louis et al. (1982)			
Atmospheric boundary process	Klemp and Wilhelmson (1978) and Deardorff (1980)			
Cloud physics	Explicit three-ice bulk microphysics (Lin et al. 1983)			
Radiation	Sugi et al. (1990)			

MOVE, MRI Ocean Variational Estimation.

than it had been beforehand. After the typhoons had passed, the water temperature had decreased from the surface to a depth of 200 m, and this decrease was attributed to upwelling occurring behind the typhoon. However, the amount by which the temperature decreased was clearly different for each of the two typhoons. The salinity within the mixed layer increased more after T1215 had passed than after T1109 had passed, even though the amount of precipitation was similar for both typhoons. The magnitude of the salinity increase was found to be related to the pre-existing salinity profile, i.e., the salinity was higher below the seasonal thermocline than near the surface before the passage of the typhoon.

The vertical water temperature profiles for T1106 (float 6429) and T1221 (6399) (Figure 6) showed that both the mixed and isothermal layers became deeper more than 100 km from the typhoon center on the right-hand side of the typhoon track when T1106 passed on 16 and 17 July 2011 and when T1221 passed on 13 and 14 October 2012. The deepening of the mixed layer led to an increase in the water temperature (compared with the water temperature before the passage) below the base of the mixed layer during and after the passage of the typhoon (after 18 July 2011 for T1106 and after 15 October 2012 for T1221). After T1221 had passed, in particular, the mixed layer became deeper than 100 m.

The vertical salinity profiles (Figure 6) showed that salinity in the mixed layer decreased after the passage of T1106. The salinity in the mixed layer was relatively high on 13 July 2011, before the typhoon passed, but decreased during and after the passage of the typhoon (after July 17), when heavy precipitation occurred. The mixed layer depth was almost the same as the isothermal depth, indicating that the effect of vertical turbulent mixing overwhelmed the effect of the precipitation. It should be noted that float 6429 was located at the eastern edge of the warm eddy on July 13 (Figure 2a), whereas it was located within the cold eddy on July 20 (Figure 2e). The westward propagation of mesoscale oceanic circulation and the resultant changes in environmental oceanic conditions possibly caused changes to occur in the temperature and salinity profiles at depth greater than 80 m before the passage of T1106.

The salinity profile of the upper ocean was quite different for T1221 than for T1106. The salinity was high in the seasonal thermocline on 10 October 2012 before T1221 passed. The salinity became low near the surface when T1106 passed over, whereas the salinity became low around the seasonal thermocline when for T1221 passed over. Figure 4 shows that the precipitation accompanying T1221 was much heavier (the three-hourly accumulated precipitation reached 1,000 mm around the location of float 6399) than the precipitation accompanying T1106, and this was caused by the relatively slow and irregular track of T1221. Water with a low salinity near the surface was transported downward by strong vertical turbulent mixing around the location of float 6399. Strong vertical turbulent mixing associated with T1221 not only deepened the mixed layer but also homogenized the water by decreasing the salinity in the lower part of the mixed layer and increasing the salinity in the upper part of the mixed layer, resulting in the water at depths of 60 to 100 m becoming fresher from October 15 to 20 (Figure 6b). A similar decrease in the salinity after the typhoon had passed was not observed

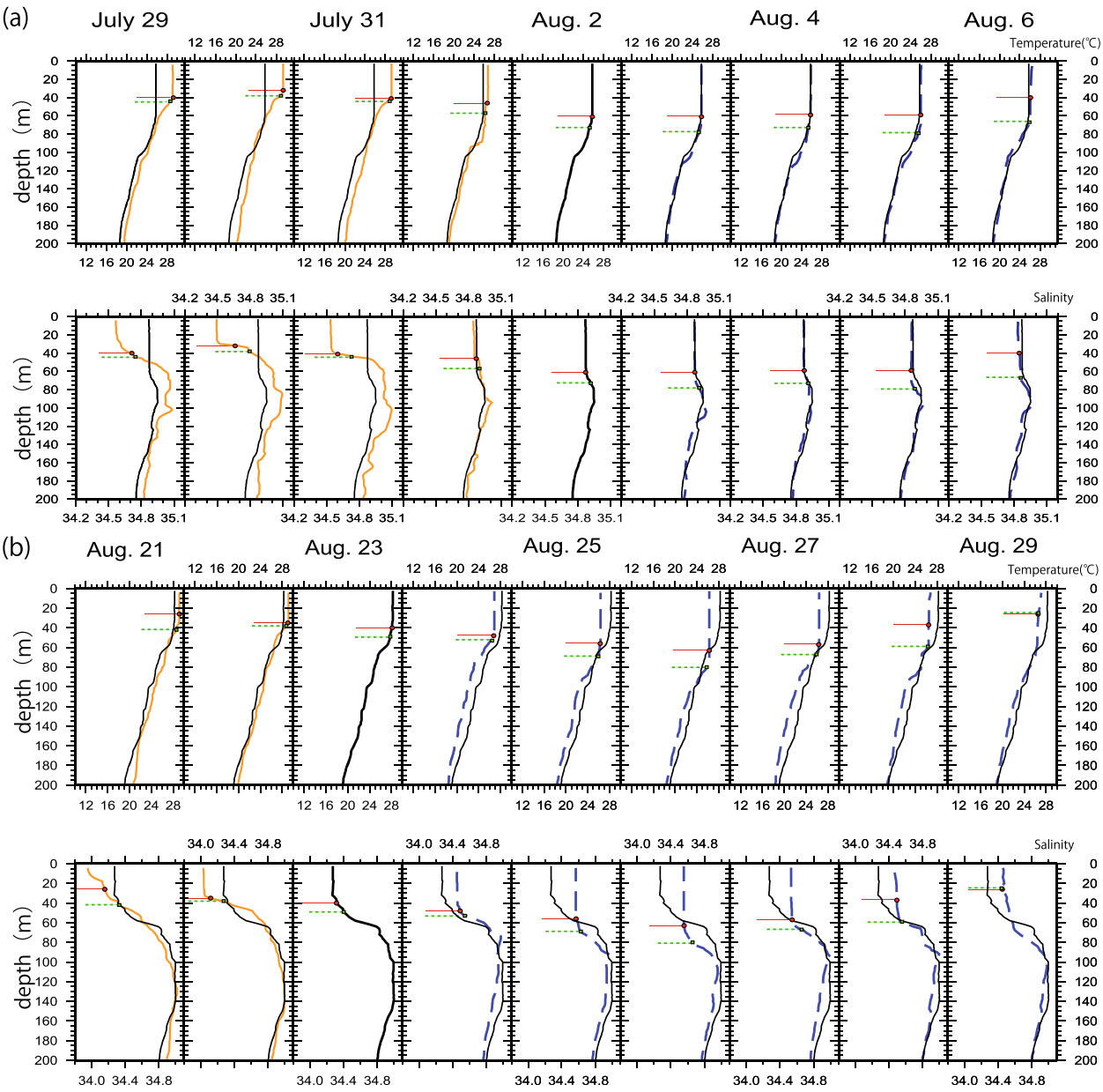

Figure 5 Vertical profiles of the water temperature and salinity in the vicinity of the typhoon track. Vertical profiles of the water temperature (upper panel) and salinity (lower panel) in the vicinity of the typhoon track during the periods **(a)** 31 July to 3 August 2011 for T1109, observed by profiling float 7560, and **(b)** 23 to 26 August 2012 for T1215, observed by profiling float 6399. Thin solid orange lines indicate the profiles before the passage of a typhoon. The thick line indicates the profile during the passage of the typhoon. Dashed blue lines indicate the profiles after the passage of a typhoon. Red circles with a solid line indicate the depth of the mixed layer. Green squares with a dashed line indicate the depth of the isothermal layer.

in the vicinity of a typhoon, less than 100 km from the center (Figure 5). The slow and irregular track of T1221 and the accompanying heavy precipitation played crucial roles in changing the vertical water temperature and salinity profiles.

The vertical water temperature profiles for T1106 (float 7560) and T1215 (float 6429) showed that both the mixed layer and isothermal layer depths more than 100 km from the typhoon center on the left-hand side of the typhoon track were deepest during the passage of T1106 on 16 July 2011 and T1215 on 24 and 25 August 2012 (Figure 7). The differences between the mixed and isothermal layer depths in T1106 and T1215 were relatively small compared with the differences between the mixed and isothermal layer depths found in the vicinity of a typhoon (Figure 5) and on the right-hand side of a

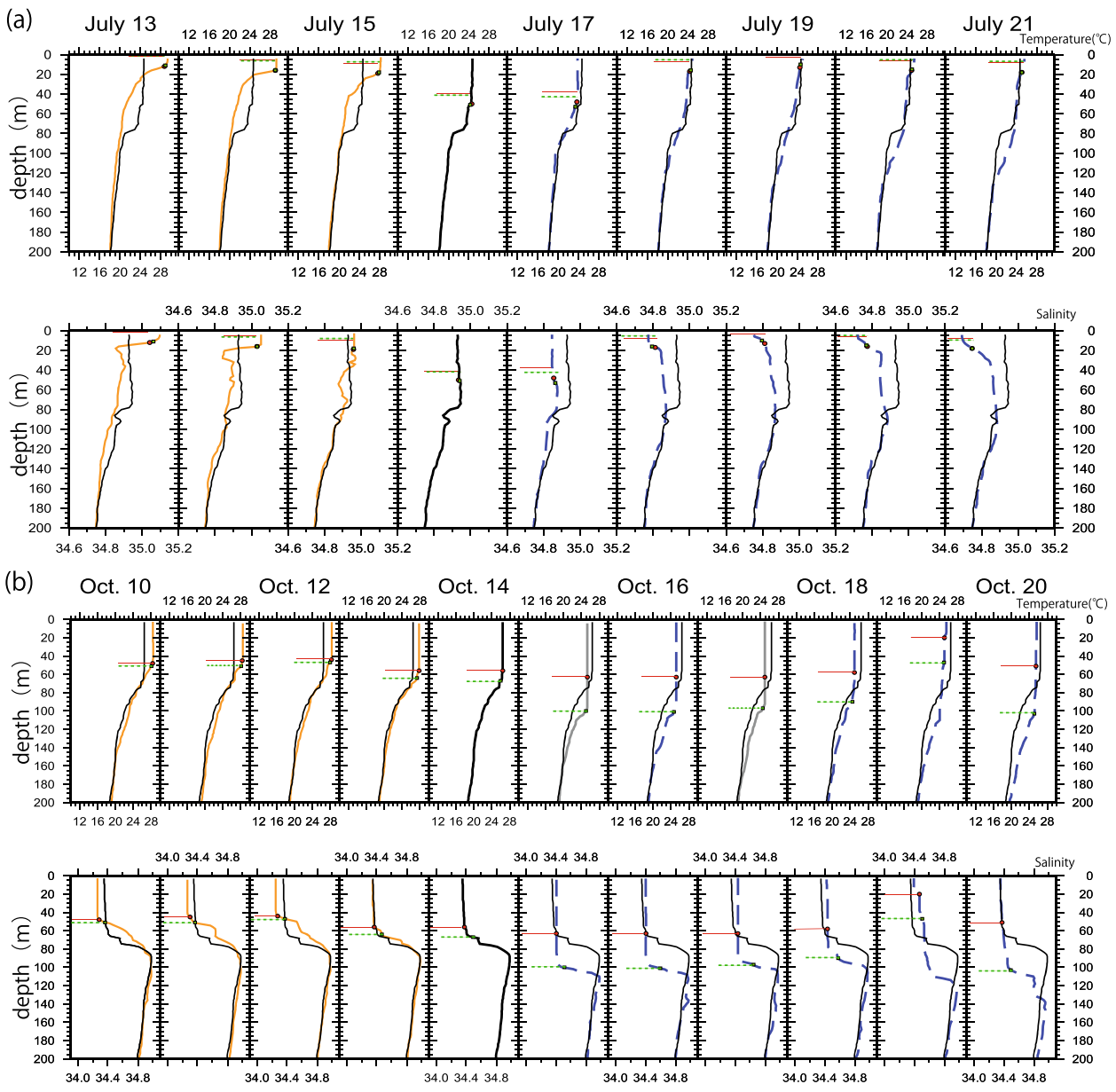

Figure 6 Vertical profiles of the water temperature and salinity on the right-hand side of the typhoon. Vertical profiles of the water temperature (upper panel) and salinity (lower panel) on the right-hand side of the typhoon, relative to its direction of motion, during the periods **(a)** 15 to 18 July 2011 for T1106, observed by profiling float 6429, and **(b)** 12 to 17 October 2012 for T1221, observed by profiling float 6399. Thin solid orange lines indicate the profiles before the passage of a typhoon. The thick line indicates the profile during the passage of the typhoon. Dashed blue lines indicate the profiles after the passage of a typhoon. Red circles with a solid line indicate the depth of the mixed layer. Green squares with a dashed line indicate the depth of the isothermal layer.

typhoon (Figure 6). Similar to the salinity profiles found more than 100 km from the center of a typhoon on the right-hand side, the vertical salinity profiles on the left-hand side showed that both the mixed layer and the isothermal layer became deeper during the passage of each typhoon. However, the salinity was lower both before and after the passage of the typhoon than during its passage, even though the total amount of precipitation was not remarkably high. Moreover, the decreases in the water temperatures caused by the passage of the typhoons were relatively small compared with the decreases found in the vicinity of a typhoon and more than 100 km from the center on the right-hand side. Figure 2 shows that vertical temperature and salinity profiles were both located over the warm core eddies. Both the mixed and isothermal layer depths were approximately 30 to

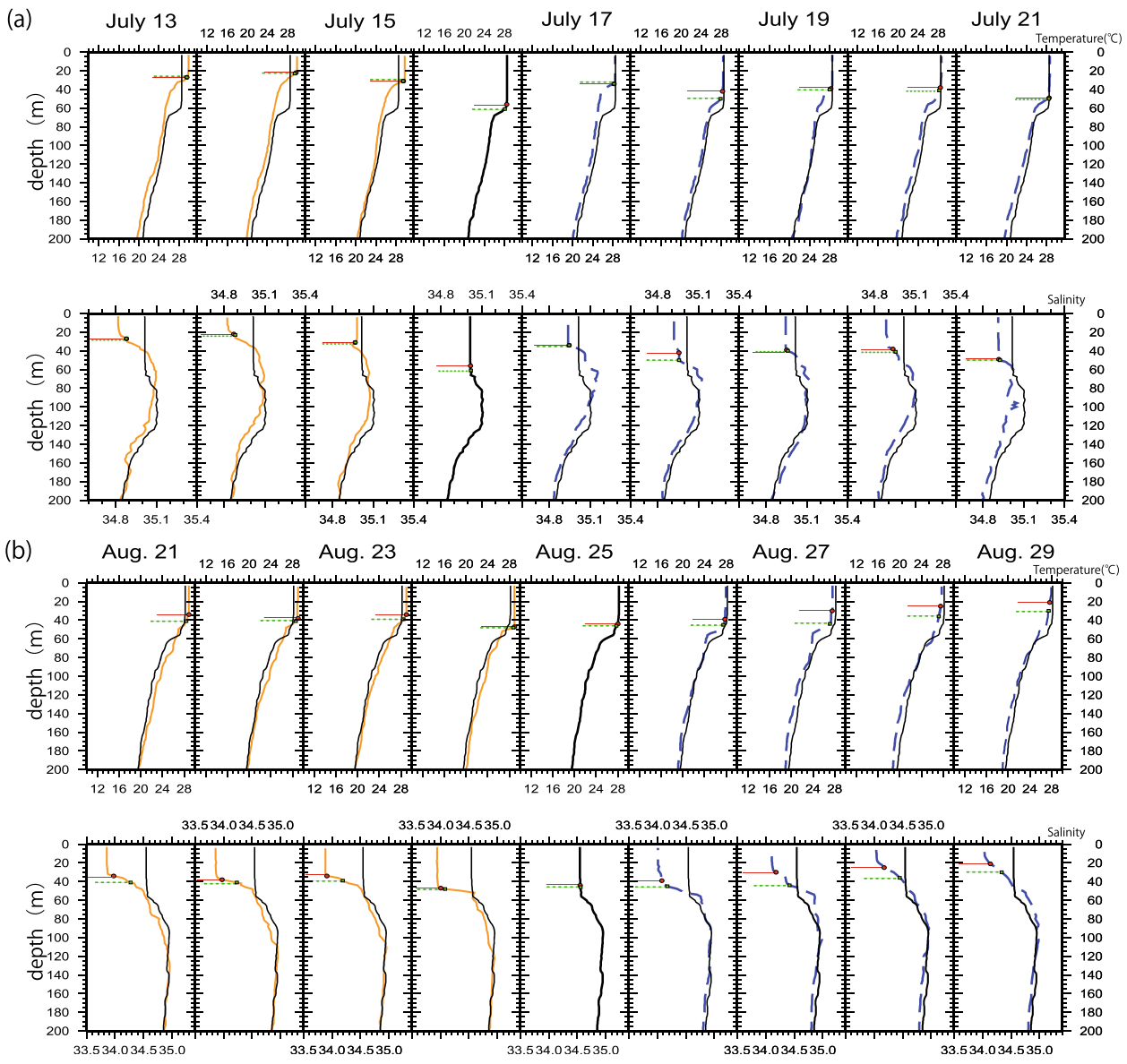

Figure 7 Vertical profiles of the water temperature and salinity on the left-hand side of the typhoon. Vertical profiles of the water temperature (upper panel) and salinity (lower panel) on the left-hand side of the typhoon, relative to its direction of motion, during the periods **(a)** 15 to 18 July 2011 for T1106, observed by profiling float 7560 and **(b)** 23 to 26 August 2012 for T1215, observed by profiling float 6429. Thin solid orange lines indicate the profiles before the passage of a typhoon. The thick line indicates the profile during the passage of the typhoon. Dashed blue lines indicate the profiles after the passage of a typhoon. Red circles with a solid line indicate the depth of the mixed layer. Green squares with a dashed line indicate the depth of the isothermal layer.

40 m, which was relatively deep compared with the depths before the passage of T1106 on 13 July 2011 and of T1215 on 21 August 2012 (Figure 7). These conditions are not favorable for the passage of a typhoon causing sea surface cooling.

Cione and Uhlhorn (2003) found differences between inner-core and ambient sea surface temperatures of approximately 0°C to 2°C. These differences are much smaller than the cold-wake-like decrease in the sea surface temperature of 4°C to 5°C, which is typically observed. Our findings were consistent with those of Cione and Uhlhorn (2003). During the passage of a typhoon, the inner-core sea surface temperature is mainly determined by vertical turbulent mixing, irrespective of the position relative to the typhoon center. In fact, the vertical water temperature and salinity profiles we found demonstrate that the mixed layer, determined from both the water temperature and the salinity, becomes deeper

almost the entire time that a typhoon passes over. However, in our analysis, we did not take into account the effect of the translation speed of the typhoon on vertical turbulent mixing, even though the translation speed is known to be important to the oceanic response to a typhoon (Lin et al. 2009) and certainly affected changes in the vertical water temperature and salinity profiles for T1221 (Figures 5b and 6b). It will be necessary to further explore the relationship between the translation speed of a typhoon and the different oceanic responses to the typhoon at different positions relative to the center.

The results of this study imply that the oceanic response to a typhoon is influenced by pre-existing oceanic conditions. In fact, Figure 2 shows that the water on the right-hand side of the tracks of some of the typhoons was much colder than the water on the left-hand side before the typhoons passed, which is confirmed by Figures 6 and 7. In that sense, the contribution of cool conditions to strong sea surface cooling is not negligible. A strong cooling effect depends, to some extent, on the location relative to the typhoon, especially when warming or cooling occurs in the seasonal thermocline; however, the cooling effect is also partly caused by differences in pre-existing oceanic vertical profiles. To explore this subject more thoroughly, many more *in situ* observations underneath typhoons, with different pre-existing oceanic conditions, will be required. That is beyond the scope of this study, but such a study should be performed in the future.

Typhoon track, central pressure, and sea surface temperature

In previous studies, sea surface cooling has been found to have led to the weakening of the typhoons themselves (Chang and Anthes 1979; Zhu et al. 2004; Wu et al. 2005; Bender et al. 2007; Wada 2009). The weakening of a typhoon means that surface wind weakened, leading to the vertical turbulent mixing in the oceanic mixed layer being modified, and this modification affecting the cooling of the sea surface. Therefore, in this subsection, we will investigate the impact of typhoon-induced sea surface cooling on the simulations of the tracks and intensities of T1106, T1109, T1215, and T1221 using the atmosphere-wave-ocean coupled model. The maximum sea surface cooling determined from the *in situ* observations exceeded 2°C for these four typhoons (Table 1). It should be noted that the maximum sea surface cooling that occurred during the other four typhoons (T1112, T1114, T1115, and T1116) could have exceeded 2°C; however, we did not assess these four typhoons because no *in situ* observational evidence that the maximum sea surface cooling exceeded 2°C was available (Table 1). The position of each simulated typhoon during the integration time was defined as the location where the sea-level pressure reached a minimum value at a certain time. The intensity of a typhoon was defined as its central pressure. The TRMM/TMI maximum sea surface cooling effects shown in Table 3 were calculated as the maximum differences between the sea surface temperature on a certain day within each analysis period (Table 1) and the sea surface temperature on the initial analysis day of that analysis period (Figure 1). The maximum sea surface cooling effect simulated using the coupled model was calculated in a similar way; however, it was the maximum difference between the sea surface temperature at a certain integration time within the entire integration period (Table 1) and the sea surface temperature at the initial time.

The RSMC-Tokyo best tracks for T1106 (Figure 8a), T1109 (Figure 8b), T1215 (Figure 8c), and T1221 (T1221L and T1221H; Figure 8d) were compared with their simulated tracks, and calculated using the NHM (uncoupled) and the full coupled atmosphere-wave-ocean models. Both of the simulated T1106 tracks showed excessive westward translation only at around 20°N and 136°E (Figure 8a). The impact of simulated sea surface cooling on the track simulation was small for T1106, and ocean coupling did not decrease the westward bias of the simulation. In contrast, the T1109 track simulated using the coupled model was closer to the best track than was the track simulated using the uncoupled model (Figure 8b). Like the T1106 track simulations, both of the T1215 and T1221 track simulations showed that simulated sea surface cooling did not significantly affect the simulated tracks of T1215 (Figure 8c), T1221L, or T1221H (Figure 8d). The T1215 tracks simulated using both the uncoupled and coupled models showed a northward bias at around 21°N and 134°E and a northwestward bias east of 132°E without changing the direction of movement to the north-northwest. The T1221 tracks simulated using both the uncoupled and coupled models showed a southward bias when the typhoon was moving westward and a northward bias around the recurvature point (20°N and 128°E) when the typhoon was moving northeastward. The translation of the simulated typhoon was relatively slow compared with the translation determined using the RSMC-Tokyo best-track data.

The differences between the tracks simulated using the uncoupled and coupled models reflected the configuration of the lateral sponge layer in the regional atmospheric model (Wada 2012). It is possible that a small number of lateral sponge layers caused the track simulation of the regional 'child' model to differ from that of the 'parent' analysis (e.g., by global objective analysis) because the effect of the parent analysis on the track simulations using the regional uncoupled and coupled models became small. In these numerical simulations, we set the sponge layer number to 70 for T1106 with 1,391 × 1,201 grids, 100 for T1109 with 1,101 × 1,101 grids, 60 for T1215 with 1,291 × 1,021 grids, and 15 for

Table 3 Maximum sea surface cooling effects

Location of float ID	T1106 (℃)	T1109 (℃)	T1215 (℃)	T1221L (℃)	T1221H (℃)
6429	4.0	2.8	3.2	3.3	3.2
7560	3.1	2.8	3.2	2.5	2.6
6399	3.0	2.6	2.7	3.9	3.9
Max. cooling (model)	5.4	3.2	3.2	2.9	3.3
Max. cooling (TMI/AMSRE)	6.3	3.9	4.8	5.7	

T1221 with 701 × 701 grids (Table 2). The sponge layer number of 70 for T1106 was comparable to the sponge layer number of 100 for T1109; thus, the differences between the tracks simulated using the coupled and uncoupled models could not be accounted for by the sponge layer number for T1109. Therefore, these results suggest that the differences between the impacts of the simulated sea surface cooling on the track simulation depended on the typhoon and the atmospheric environments. Later in this subsection, we will investigate the impact of ocean coupling on the track simulation of T1109 further.

The central pressure time series for T1106 (Figure 9a), T1109 (Figure 9b), T1215 (Figure 9c), and T1221 (T1221L and T1221H; Figure 9d) simulated using the uncoupled and coupled models were compared with the time series for the RSMC-Tokyo best-track central pressures for each typhoon. The intensification, mature, and decaying phases for all of the typhoons except for T1215, which includes only the intensification phase according to the best-track data, are shown in Figure 9.

The simulated sea surface cooling induced by the typhoon began to have an impact on the simulated central pressure during the intensification phase for all four typhoons. The central pressures for T1106 (Figure 9a) and T1221 (Figure 9d) simulated using the uncoupled model were lower than the RSMC-Tokyo best-track central pressures, particularly during the mature phase. The

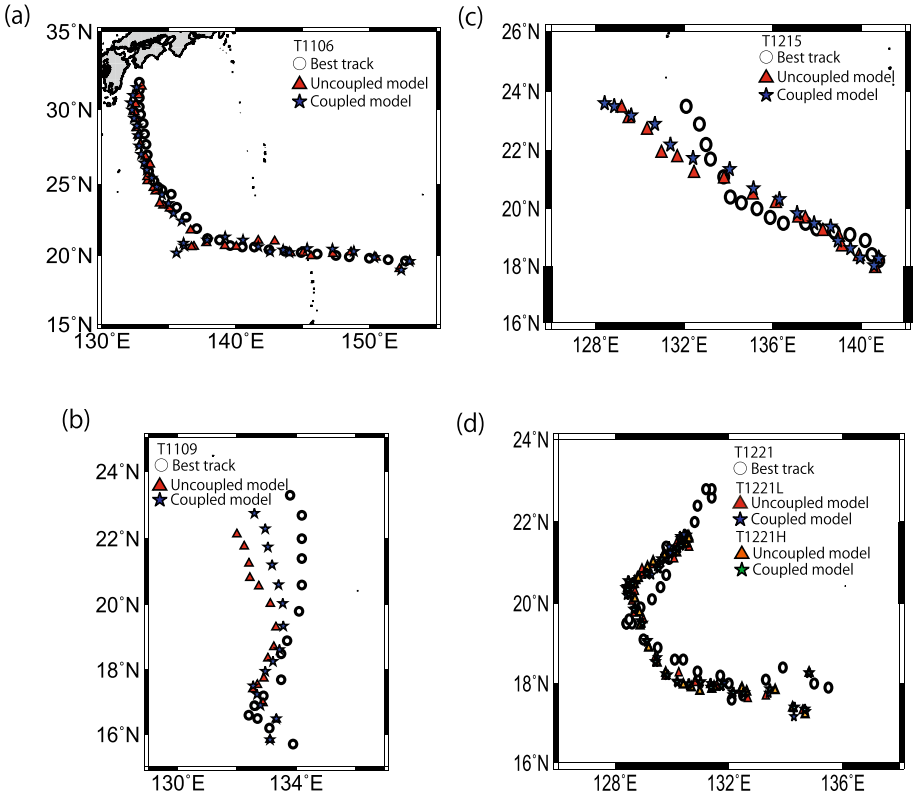

Figure 8 RSMC-Tokyo best tracks and simulated best tracks. (a) T1106, **(b)** T1109, **(c)** T1215, and **(d)** T1221L and T1221H.

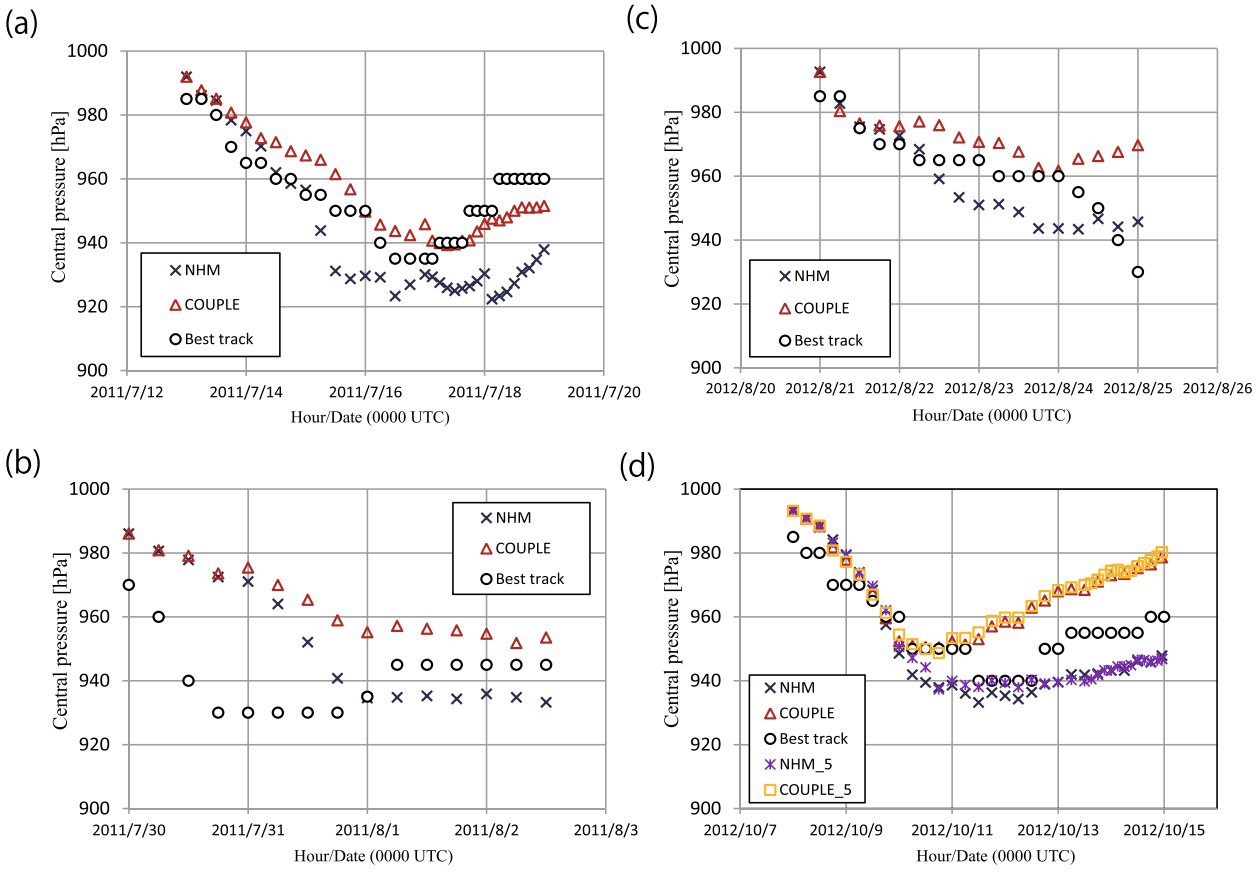

Figure 9 Time series of the RSMC-Tokyo best-track central pressures and simulated central pressures. (a) T1106, **(b)** T1109, **(c)** T1215, and **(d)** T1221L and T1221H. Open circles indicate RSMC-Tokyo best-track central pressures.

central pressure for T1215 (Figure 9c) simulated using the coupled model was lower than the RSMC-Tokyo best-track central pressure at around 0000 UTC on 25 August 2011 during the rapid intensification phase. This low central pressure was caused by an error in the track simulation (Figure 8c). During the intensification phase, in contrast, the central pressures simulated using the uncoupled model were much higher than the best-track central pressures for T1109 (Figure 9b). The central pressures simulated using the coupled model were higher than the central pressures simulated using the uncoupled model for all of the typhoons. This result, which shows that the simulated sea surface cooling induced by the typhoons decreased the magnitude of the TC intensification and the final (maximum) intensity, is consistent with the results of previous studies (Bender et al. 1993; Shade and Emanuel 1999; Wada 2009). This negative-feedback effect, however, did not improve the central pressure simulations, particularly in the rapid intensification phase, for the typhoons that were studied.

In addition, the impact of the horizontal resolution of the MOVE data on both the track (Figure 8d) and central pressure simulations for T1221 was small (T1221L and T1221H; Table 2 and Figure 9d). This is also consistent with previous findings (Wada et al. 2013). This suggests that the impact of the horizontal resolution difference in the oceanic analysis data on the typhoon simulation was negligible.

The horizontal sea surface temperature distributions used in the uncoupled model (Figure 10a,b,c,d,e) were compared with the distributions simulated using the coupled model (Figure 10f,g,h,i,j) for T1106 at 120 h, T1109 at 84 h, T1215 at 96 h, and T1221L and T1221H at 120 h. The sea surface temperature differences between the simulations using the uncoupled and coupled models are shown in Figure 11. The horizontal sea surface temperature distributions used in the uncoupled model did not change during the integration period. The results of the simulations using the coupled model revealed that sea surface cooling was induced by T1106 (Figures 10f and 11a), T1109 (Figures 10g and 11b), and T1215 (Figures 10h and 11c) on the right-hand side of the simulated track. The horizontal sea surface temperature distributions for T1221 were greatly changed by ocean coupling because of the simulated recurved irregular tracks with a slow translation. However, even using the

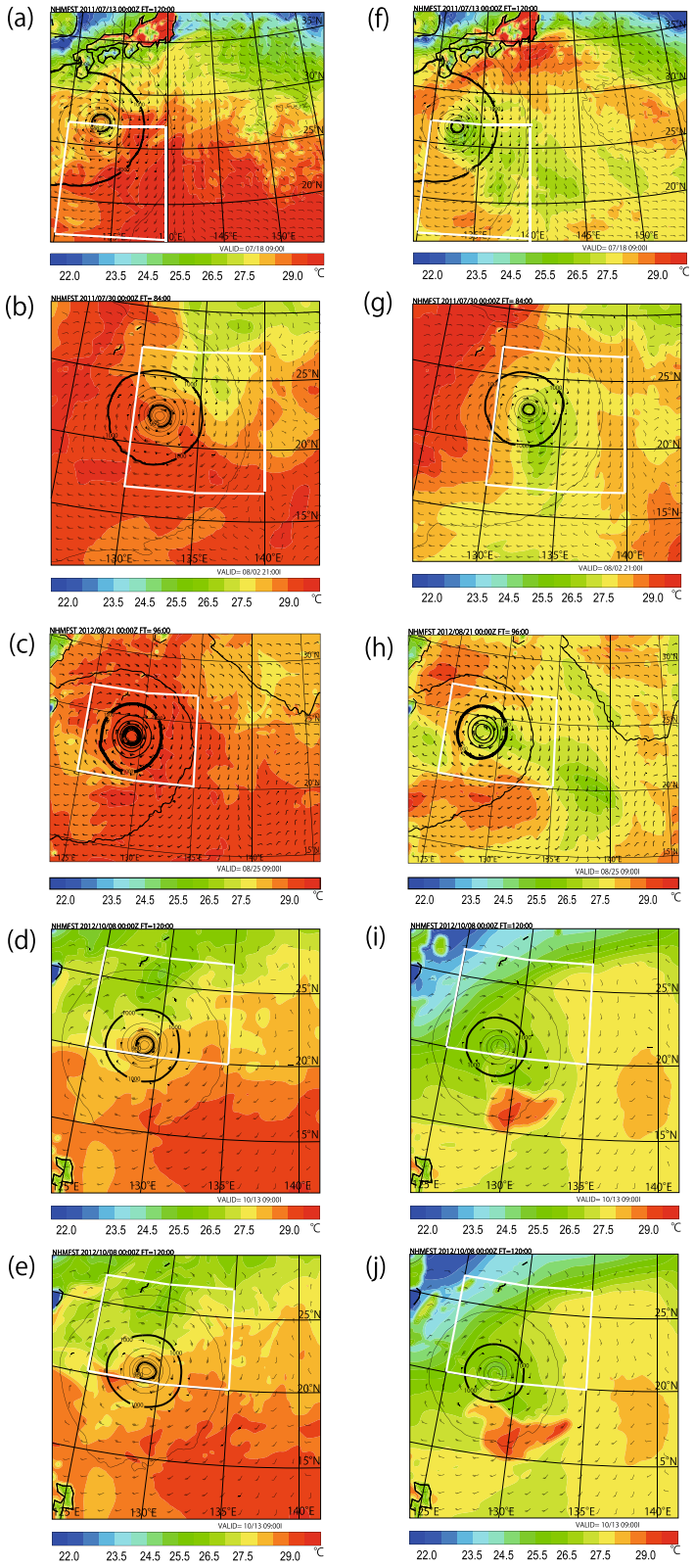

Figure 10 (See legend on next page.)

(See figure on previous page.)

Figure 10 Horizontal distributions of the sea surface temperature, sea-level pressure, and wind. Horizontal distributions of the sea surface temperature (color shading), sea-level pressure (contours; contour intervals are 8 hPa (thin line) and 40 hPa (thick line)), and wind at the 850 hPa level (vectors) simulated using **(a** to **e)** the uncoupled model and **(f** to **j)** the coupled model for (a and f) T1106, (b and g) T1109, (c and f) T1215, (d and i) T1221L, and (e and j) T1221H. White boxes indicate the domains wherein the three profiling floats were monitored (see Figure 1).

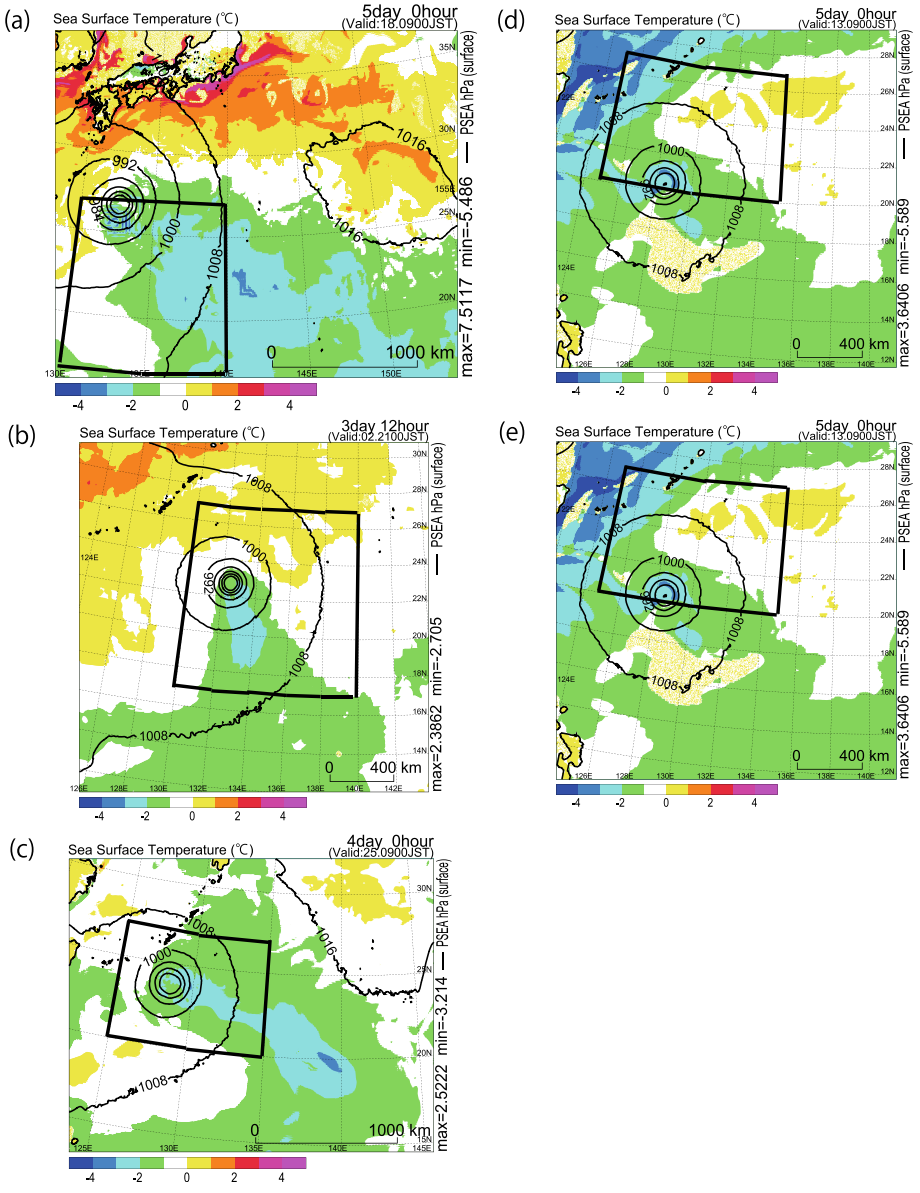

Figure 11 Horizontal distributions of the differences in sea surface temperatures simulated using the uncoupled model. Horizontal distributions of the differences in sea surface temperatures (color shading; the sea surface temperature simulated using the uncoupled model subtracted from the sea surface temperature simulated using the coupled model), and sea-level pressures simulated using the coupled model (contours; contour intervals are 8 hPa) **(a)** at 120 h for T1106, **(b)** at 84 h for T1109, **(c)** at 96 h for T1215, **(d)** at 120 h for T1221L, and **(e)** at 120 h for T1221H. Black boxes indicate the domains wherein the three profiling floats were monitored (see Figure 1).

coupled model (Figure 10i,j), the sea surface temperatures in the simulation (Table 3) were high compared with the observations (Table 1). The difference between the sea surface temperatures in T1221 that were observed in the simulations using the uncoupled and coupled models was relatively small compared with that for the other typhoons.

It is difficult to compare the simulated sea surface temperature with the TRMM/TMI sea surface temperature at a certain point/grid because of errors in the track and intensity simulations. Therefore, we compared the horizontal simulated sea surface temperature distributions (Figure 10f,g,h,i,j) and the differences between the simulations using the uncoupled and coupled models (Figure 11) with those for the TRMM/TMI sea surface temperatures (Figure 3e,f,g,h), and the differences between before and after the typhoon had passed (Figure 3i,j,k,l). Sea surface cooling clearly occurred on the right-hand side of the track for T1106, T1109, and T1215, which is consistent with the numerical simulation results (Figures 10 and 11). TRMM/TMI sea surface cooling on the right-hand side of the track was not remarkable for T1221 (Figure 3h). This characteristic was simulated reasonably well by the coupled model (Figures 10g,h, and 11d,e).

Compared with the TMI/AMSRE microwave satellite observations (Table 3), the simulated maximum sea surface cooling effects, 5.4°C for T1106, 2.7°C for T1109, 3.2°C for T1215, 2.9°C for T1221L, and 3.3°C for T1221H, were relatively low, indicating that a relatively high sea surface temperature was simulated by the coupled model. This relatively low sea surface cooling effect was attributed to the weakened vertical turbulent mixing caused by the high central pressures (causing a weak intensity) simulated using the coupled model (Figure 9). If the simulated sea surface cooling effect had been close to the TRMM/TMI sea surface cooling effect, the typhoon intensity would have been further weakened because of excessive cooling. This implies that the air-sea enthalpy fluxes within the inner core of a simulated typhoon were insufficient to simulate intensification and the maximum intensity of the typhoon. In other words, much higher enthalpy fluxes from the ocean to the atmosphere are needed, particularly within the inner core, to simulate the intensification phase and the maximum intensity.

Next, we explored the impact of sea surface cooling induced by T1109 on the difference between the tracks simulated using the uncoupled and coupled models. Figure 12 shows the deviations in equivalent potential temperatures at the 200 hPa level and wind velocities at the 500 hPa level that were simulated using the coupled and uncoupled models (the uncoupled results subtracted from the coupled results) for T1109. The typhoon-induced sea surface cooling effect led to a decrease in the equivalent potential temperature within the inner warm core of the typhoon at the 200 hPa level at 36 h (Figure 12a). This decrease caused anticyclonic circulation anomalies, which helped suppress cyclonic circulation, at the 500 hPa level in the center of the typhoon.

A decrease in the equivalent potential temperature was also apparent around the rainband on the western side of the typhoon center after 36 h (data not shown). In contrast, the equivalent potential temperature at the 200 hPa level at 42 h increased east of the area where the decrease occurred (Figure 12b). This warming was accompanied by enhanced cyclonic circulation at the 500 hPa level.

The difference in the equivalent potential temperatures between the uncoupled and coupled models at 60 h had a wavenumber-1 asymmetric structure (Figure 12c), indicating that the difference between the tracks simulated using the uncoupled and coupled models was significant. The increases in the equivalent potential temperatures at the 200 hPa level occurred on a mesovortex scale at 42 h, and the mesovortices coalesced at 60 h, strengthening the cyclonic circulation. This enhanced cyclonic circulation enabled the location of the center of the simulated typhoon to move despite the sea surface cooling that occurred beneath the typhoon.

In general, differences between the typhoon tracks simulated using the uncoupled and coupled models were small because of the competing processes associated with the changes in typhoon asymmetry and changes in the beta drift, which is a drift attributed to the background potential vorticity represented by the meridional gradient of the Coriolis parameter β, caused by ocean coupling under relatively weak background flow (Bender et al. 1993; Wu et al. 2005). Figure 13a shows the depth-weighted steering flows for T1106, T1109, T1215, T1221L, and T1221H simulated using the coupled model. The depth-weighted steering flow was calculated as a mass-weighted average every 3 h using the winds and geopotential heights at pressure levels between 300 and 850 hPa from the center of the typhoon to a radius of 400 km. The easterly steering flow was dominant in all of the typhoons except for T1109. However, the direction of the steering flow was southwesterly for T1109, and the magnitude of the steering flow was relatively small. The impact of ocean coupling on the depth-weighted steering flow was not negligible for T1109 because the magnitude of the zonal depth-weighted steering flow was less than 2 m s^{-1} (Figure 13b). The magnitude of the zonal depth-weighted steering flow for T1109 was quite different from that for T1215. Therefore, the weakening of both the typhoon intensity and the outer wind speeds caused the steering flow to change toward the northeast. In other words, more westward tracks simulated using the uncoupled model after 48 h may have been caused by northwestward beta

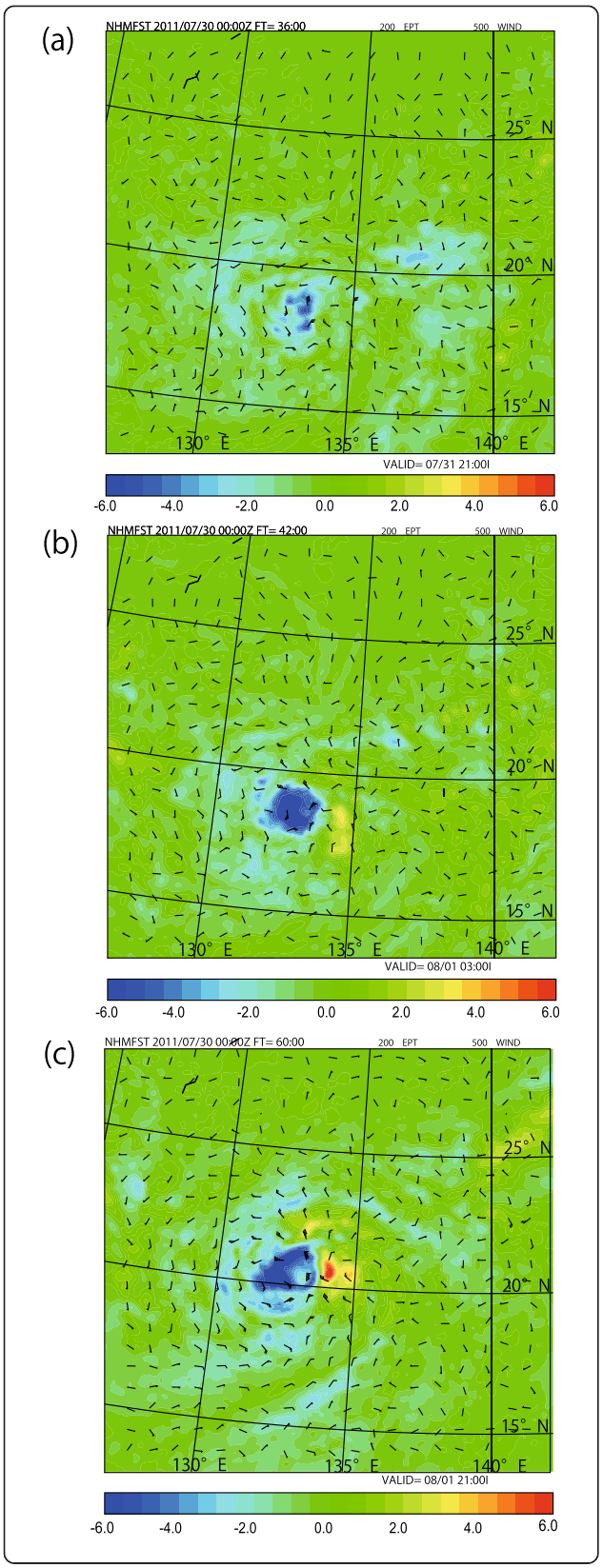

Figure 12 Differences in equivalent potential temperatures and wind simulated using uncoupled and coupled models. Differences in the 200 hPa equivalent potential temperatures (color shading) and 500 hPa wind (vectors) simulated using the uncoupled and coupled models (uncoupled results subtracted from the coupled results) for T1109 at **(a)** 36 h, **(b)** 42 h, and **(c)** 60 h.

drift under a relatively strong vortex and weak zonal basic flow. If the rapid intensification of T1109 had been successfully simulated the simulated track would have had a more northwestward bias. However, the larger amount of typhoon-induced sea surface cooling (see Table 3) would have changed the bias from northwestward to northeastward. This suggests that ocean coupling has the potential to improve track predictions under relatively weak basic flow.

Simulated sea surface cooling and latent heat fluxes

From the viewpoint of dynamics, sea surface cooling beneath a typhoon plays an essential role in delaying the merger of mesovortices within the inner core (Wada 2009). From the viewpoint of thermodynamics, typhoon-induced sea surface cooling leads to decreases in the latent heat fluxes from the ocean to the atmosphere. In this subsection, we will assess how typhoon-induced sea surface cooling affects the typhoon from the viewpoints of both dynamics and thermodynamics. Because latent heat fluxes are much higher than sensible heat fluxes over the ocean, we will focus on latent heat fluxes within the inner core of a typhoon, the inner core being defined as the region from the center of the typhoon to a radius of 200 km.

We will consider the axisymmetrical mean profiles of the sea surface temperature and the latent heat flux within the inner core at 24, 48, and 72 h, because the axisymmetric sea surface cooling effect during the intensification phase plays a decisive role in weakening the typhoon intensity, despite its relatively small magnitude compared with the asymmetric component of sea surface cooling after the passage of the typhoon (Wu et al. 2005). The three integration times we will use correspond to the intensification or mature phases of the typhoons we studied, except for T1221, which was transitioning from the mature phase to the decaying phase at 72 h. The bin sizes used when calculating the axisymmetrical mean values were 4 km for T1106, T1109, and T1215, and 6 km for T1221L and T1221H.

Tables 4 and 5 show the maximum values of the axisymmetrical mean latent heat fluxes calculated using the uncoupled and coupled models, and the maximum sea surface cooling derived from the deviations in the axisymmetrical mean sea surface temperatures between the uncoupled and coupled models at 24, 48, and 72 h for T1106, T1109, T1215, T1221L, and T1221H. The latent

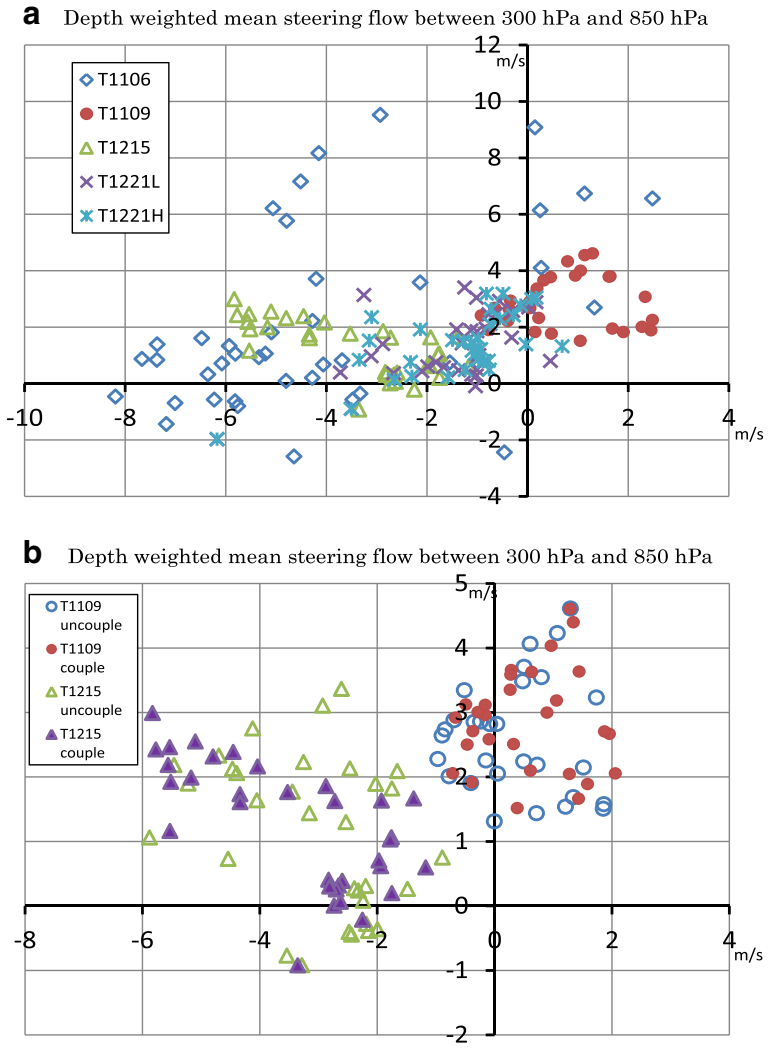

Figure 13 Scatter diagrams of the depth weighted mean steering flows. (a) Simulated using the coupled model for T1106 (open diamonds), T1109 (close circles), T1215 (open triangles), T1221L (crosses), and T1221H (asterisks). **(b)** Simulated using the uncoupled model (open marks) and coupled model (closed marks) for T1109 (circles) and T1215 (triangles). Positive values in the azimuthal axis indicate westerly steering flows, and positive values in the vertical axis indicate southerly steering flows.

heat fluxes calculated using the uncoupled model ranged from 275.1 W m^{-2} (for T1221L at 24 h) to 713.4 W m^{-2} (for T1215 at 48 h), whereas the latent heat fluxes calculated using the coupled model ranged from 209.4 W m^{-2} (for T1221L at 24 h) to 484.1 W m^{-2} (for T1215 at 72 h). The ratio of the latent heat flux calculated using the coupled model to the latent heat flux calculated using the uncoupled model ranged from 0.53 to 0.76. This implies that the latent heat fluxes were decreased by 24% to 47% due to ocean coupling, including the typhoon-induced sea surface cooling effect. Interestingly, the ratio decreased as the maximum sea surface cooling increased. For example, the highest maximum sea surface cooling effect was 1.8°C for T1109 at 48 h; however, the ratio for T1109 (0.53) at that time was the lowest of the typhoons that were studied (Tables 4 and 5), which means that latent heat flux was decreased by 47%. The ratio tended to be relatively high during the intensification phase (e.g., 0.76 at 24 h for T1221L that is a decrease of only 24%), when the sea surface cooling effect was relatively small (0.5°C at 24 h for T1221L).

At 48 h, when the sea surface cooling effect for T1109 was at its greatest (Tables 4 and 5), the maximum sea surface cooling effect tended to occur where the axisymmetrical mean sea surface temperature from the center of the typhoon to a radius of 200 km was at its lowest (Figure 14a). Moreover, the radial profile of the standard deviation of the axisymmetrical mean sea surface temperature indicated that the response of the sea surface temperature was asymmetrical outward along the

Table 4 Axisymmetrical mean latent heat fluxes and sea surface cooling effects for T1106 and T1109

Integration time	T1106			T1109		
	Latent heat flux (uncoupled; W m^{-2})	Latent heat flux (coupled; W m^{-2})	Sea surface cooling (°C)	Latent heat flux (uncoupled W m^{-2})	Latent heat flux (coupled; W m^{-2})	Sea surface cooling (°C)
24 h	451.9	324.2	1.0	331.1	227.5	1.0
(Ratio)		0.72			0.69	
48 h	459.0	266.8	1.5	569.9	303.3	1.8
(Ratio)		0.58			0.53	
72 h	566.4	388.3	1.2	492.9	260.6	1.6
(Ratio)		0.69			0.53	

radius of the maximum sea surface cooling effect. This is consistent with the asymmetry (rightward bias) seen in the oceanic response to typhoons in the Northern Hemisphere. In contrast, the radial profile of the standard deviation of the axisymmetrical mean latent heat flux hardly showed any asymmetry (Figure 14b) because the primary circulation of a typhoon is axisymmetric. The decrease in the wind speed within the inner core also played an essential role in decreasing the latent heat flux within the inner core.

We will now assess the impact of a decrease in the latent heat flux on the structure of the inner core of T1109, focusing on the lower troposphere, from the surface to 3,000 m. Changes in the latent heat flux within the inner core led to changes in the axisymmetrical mean equivalent potential temperature, the specific humidity, and the radial wind velocity. The vertical structure of the axisymmetrical mean equivalent potential temperature for T1109 showed a relatively high temperature around the center, which was a sharp horizontal temperature gradient around a radius of 50 km from the center above 1,000 m at 48 h (Figure 15a). The vertical structure of the axisymmetrical mean specific humidity showed that the specific humidity was highest around the center of the typhoon below 1,250 m, whereas it was highest at approximately 50 km from 1,250 to 3,000 m (Figure 15a). Below 1,250 m, the radial inflow was dominant from the surface to approximately 750 m, indicating the existence of an inflow boundary layer (Barnes and Powell 1995; Kepert and Wang 2001). The standard deviations were relatively low within the inflow boundary layer (Figure 15). This indicates that the primary circulation was axisymmetrically dominant in that area.

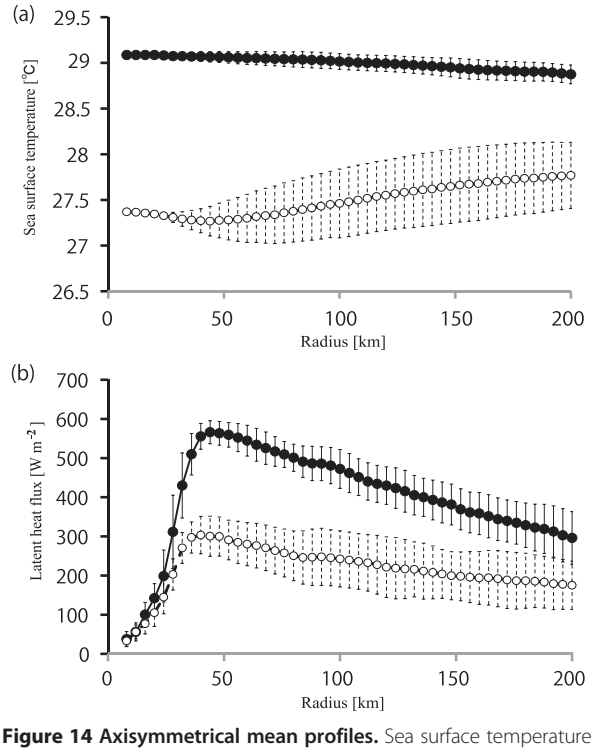

Figure 14 Axisymmetrical mean profiles. Sea surface temperature **(a)** and latent heat flux **(b)**, with standard deviations, for T1109 at 48 h. Closed circles with solid lines indicate the results simulated using the uncoupled model and open circles with dashed lines indicate the results simulated using the coupled model.

A decrease in the latent heat flux at 48 h led to a decrease in the axisymmetrical mean equivalent potential temperature around the center of the typhoon, weakening the horizontal gradient around a radius of 50 km from the center and slightly shifting outward the area wherein the standard deviation of the temperature was high (Figure 15c). The decrease caused by sea surface cooling led to a decrease in the specific humidity, particularly around a radius of 50 km in the inflow boundary layer (Figure 15d). In fact, the radial inflow simulated using the coupled model (Figure 15d) was much weaker than the radial inflow simulated using the uncoupled model (Figure 15b). This suggests that secondary circulation within the inner core of the simulated T1109 was weakened by a decrease in the latent heat flux caused by sea surface cooling induced by T1109.

Even though a sophisticated atmosphere-wave-ocean coupled model was used for the typhoon simulations, the track (Figure 8) and intensity (Figure 9) simulations

Table 5 Axisymmetrical mean latent heat fluxes and sea surface cooling effects for T1215, T1221L, and T1221H

Integration time	T1215			T1221L			T1221H		
	Latent heat flux (uncoupled; W m^{-2})	Latent heat flux (coupled; W m^{-2})	Sea surface cooling (°C)	Latent heat flux (uncoupled; W m^{-2})	Latent heat flux (couple; W m^{-2})	Sea surface cooling (°C)	Latent heat flux (uncoupled; W m^{-2})	Latent heat flux (coupled; W m^{-2})	Sea surface cooling (°C)
24 h	596.3	402.5	1.3	275.1	209.4	0.5	302.6	219.8	0.6
(Ratio)		0.67			0.76			0.73	
48 h	713.4	415.3	1.7	401.1	283.2	1.0	409.9	245.4	1.0
(Ratio)		0.57			0.71			0.60	
72 h	690.1	484.1	1.0	395.3	213.6	1.5	409.9	247.6	1.4
(Ratio)		0.67			0.54			0.60	

were not necessarily improved. In particular, rapid intensification in T1109 and T1215 was not successfully simulated even when the horizontal resolution was 2 km. Much higher enthalpy fluxes from the ocean to the atmosphere could be realized in the coupled model by introducing sea spray parameters (e.g., Bao et al. 2000), for example. Not only fine horizontal resolution but also improvements in the atmospheric physics used in the atmosphere model will be required to improve the typhoon predictions. In addition, uncertainties still remain in the initial and lateral boundary conditions in the atmosphere and ocean in the typhoon simulations.

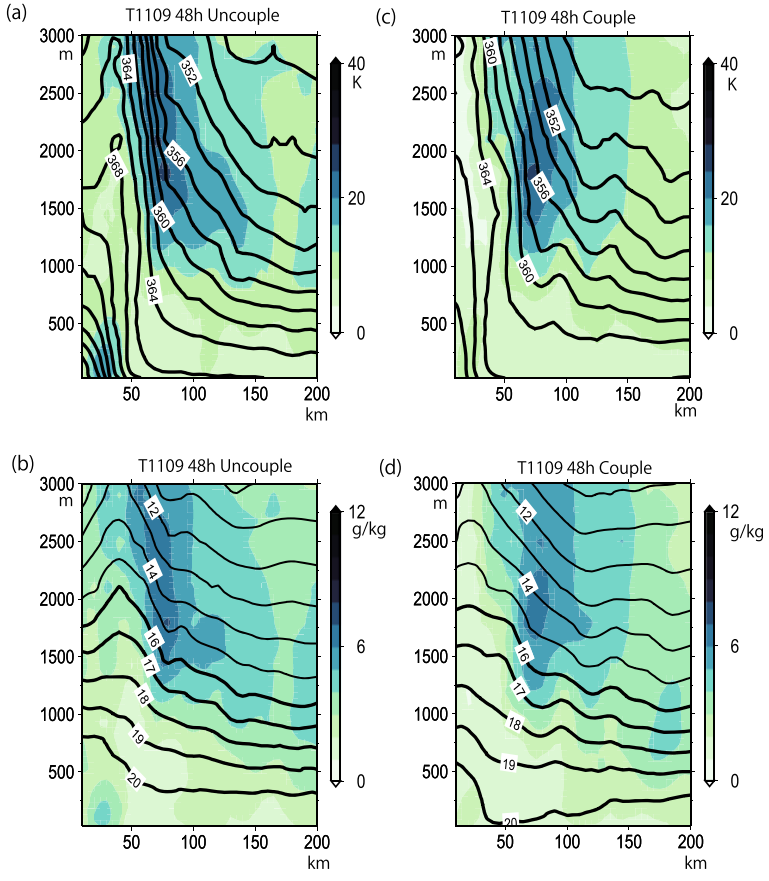

Figure 15 Axisymmetrical mean vertical profiles. (a) Equivalent potential temperature (solid contours) with the standard deviation (shaded), **(b)** specific humidity (solid contours) with the standard deviation (shaded) and radial inflow (dashed contours) simulated using the uncoupled model, **(c)** equivalent potential temperature (solid contours) with the standard deviation (shaded), and **(d)** specific humidity (solid contours) with the standard deviation (shaded) and radial inflow (dashed contours) simulated using the coupled model.

Solving these modeling problems will help clarify the mechanism involved in typhoon-induced sea surface cooling.

Conclusions

Daily observations using three profiling floats deployed around 20°N, 22°N, and 24°N along the 137°E meridian by the R/V Keifu Maru captured typhoon-induced sea surface cooling measurements during the 2011 and 2012 typhoon seasons. In this study, we investigated the characteristics of sea surface cooling effects from the viewpoint of different positions relative to the centers of the typhoons and different times through the passage of the typhoons, although sea surface cooling was partly attributed to pre-existing oceanic conditions and precipitation accompanying the typhoons. The impacts of sea surface cooling on typhoon simulations using the atmosphere-wave-ocean coupled model were assessed, focusing on the tracking and intensities of the typhoons, decreases in latent heat fluxes within the inner cores of simulated typhoons accompanying simulated sea surface cooling, and structural changes in the inner cores. The main conclusions are given below:

1. The oceanic response to a typhoon was examined according to the position of the float relative to the best-track typhoon center. Even though the oceanic response was affected by pre-existing oceanic conditions, precipitation accompanying the typhoon, the typhoon intensity, and the translation speed, the oceanic response clearly differed depending on the relative position studied. Upwelling was found to be dominant in the vicinity of the typhoon center, and the water temperature decreased from the surface to 200-m deep after the passage of a typhoon. Vertical turbulent mixing led to warming in the seasonal thermocline on the right-hand side of the typhoon track at a distance of 100 km or more from the typhoon center, whereas the oceanic response caused by vertical turbulent mixing was relatively weak on the left-hand side. Changes in the observed salinity profiles clearly differed from the changes in observed temperature profiles near the surface both before and after the passage of a typhoon in the vicinity of the center of the typhoon and on the right-hand side. This was found to be caused by stratification caused by the precipitation that accompanies typhoons and upwelled saline water in the seasonal thermocline. Deepening of the mixed layer caused by vertical turbulent mixing was clearly apparent in the temperature and salinity profiles during the passage of a typhoon.
2. Numerical simulations of typhoons Ma-on (T1106), Muifa (T1109), Bolaven (T1215), and Prapiroon (T1221) showed that typhoon-induced sea surface cooling significantly affected the extent to which simulated central pressures increased during the intensification and mature phases of the typhoons. Sea surface cooling also affected the track simulation of T1109 under weak basic flow because the weakened typhoon intensity altered the beta effect and changed the depth-weighted steering flows. Sea surface cooling beneath a typhoon led to axisymmetrical decreases in the latent heat fluxes of 24% (in the intensification phase, with sea surface cooling of less than 1°C) to 47% (in the mature phase, with sea surface cooling of more than 1°C). The decreases in the latent heat fluxes led to changes in the inner core structure of T1109, particularly in the inflow boundary layer and around the eye and eyewall, through changes in secondary circulation.

Abbreviations

AMSRE: Advanced Microwave Scanning Radiometer-Earth observing system; AVISO: Archiving: Validation and Interpretation of Satellite Oceanographic data; ID: Identification number; JMA: Japan Meteorological Agency; MOVE: Meteorological Research Institute Ocean Variational Estimation; MRI: Meteorological Research Institute; NHM: Nonhydrostatic atmosphere model; NOAA: National Oceanic and Atmospheric Administration; RSMC-Tokyo: Regional Specialized Meteorological Center-Tokyo; TC: Tropical cyclone; TMI: Tropical rainfall measuring mission microwave imager; WMO: World Meteorological Organization.

Competing interests

The authors declare that there are no conflicts of interests regarding the publication of this article.

Authors' contributions

AW proposed the topic and conceived and designed the study, including the numerical simulations using an atmosphere-wave-ocean coupled model. TU was in charge of the analysis of the profiling float data. SI conducted the oceanic reanalysis for the numerical simulations. All authors read and approved the final manuscript.

Authors' information

AW is a senior researcher in the Typhoon Research Department of the Meteorological Research Institute. TU and SI are technical officers in the Japan Meteorological Agency.

Acknowledgements

All authors would like to thank two anonymous reviewers for their thorough and helpful reviews. All authors are grateful to colleagues for observational and analysis support. This work was funded by KAKENHI Grant Number 25106708 from MEXT.

Author details

[1]Meteorological Research Institute, Japan Meteorological Agency, 1-1 Nagamine, Tsukuba, Ibaraki 305-0052, Japan. [2]Japan Meteorological Agency, 1-3-4 Otemachi, Chiyoda, Tokyo 100-8122, Japan.

Received: 2 December 2013 Accepted: 29 May 2014
Published: 10 June 2014

References

Akima H (1970) A new method of interpolation and smooth curve fitting based on local procedures. J Assoc Comp Mach 17:589–602

Bao JW, Wilczak JM, Choi JK, Kantha LH (2000) Numerical simulations of air–sea interaction under high wind conditions using a coupled model: a study of hurricane development. Mon Weather Rev 128:2190–2210, doi: http://dx.doi.org/10.1175/1520-0493(2000)128<2190:NSOASI>2.0.CO;2

Baranowski DB, Flatau PJ, Malinowski SP (2011) Tropical cyclone turbulent mixing as observed by autonomous oceanic profilers with the high repetition rate. J Phys Conf Ser 318:072001, doi:10.1088/1742-6596/318/7/072001

Barnes GM, Powell MD (1995) Evolution of the inflow boundary layer of Hurricane Gilbert (1988). Mon Weather Rev 123:2348–2368, doi: http://dx.doi.org/10.1175/1520-0493(1995)123<2348:EOTIBL>2.0.CO;2

Bender MA, Ginis I, Kurihara Y (1993) Numerical simulations of the tropical cyclone-ocean interaction with a high-resolution coupled model. J Geophys Res 98:23245–23263, doi:10.1029/93JD02370

Bender MA, Ginis I, Tuleya R, Thomas B, Marchok T (2007) The operational GFDL coupled hurricane-ocean prediction system and a summary of its performance. Mon Weather Rev 135:3965–3989, doi: http://dx.doi.org/10.1175/2007MWR2032.1

Chang SW, Anthes RA (1979) The mutual response of the tropical cyclone and the ocean. J Phys Oceanogr 9:128–135, doi: http://dx.doi.org/10.1175/1520-0485(1979)009<0128:TMROTT>2.0.CO;2

Chen SS, Price JF, Zhao W, Donelan MA, Walsh EJ (2007) The CBLAST-Hurricane program and the next generation fully coupled atmosphere-wave-ocean models for hurricane research and prediction. Bull Am Meteorol Soc 88:311–317, doi:10.1175/BAMS-88-3-311

Chen SS, Zhao W, Donelan MA, Tolman HL (2013) Directional wind-wave coupling in fully coupled atmosphere-wave-ocean models: results from CBLAST-Hurricane. J Atmos Sci 70:3198–3215, doi:10.1175/JAS-D-12-0157.1

Cione JJ, Uhlhorn EW (2003) Sea surface temperature variability in hurricanes: implication with respect to intensity change. Mon Weather Rev 131:1783–1796, doi: http://dx.doi.org/10.1175//2562.1

D'Asaro E, Black P, Centurioni L, Harr P, Jayne S, Lin I-I, Lee C, Morzel J, Mrvaljevic R, Niiler P, Sanford T, Tang T (2011) Typhoon-ocean interaction in the western North Pacific: part 1. Oceanography 24:24–31, doi:10.5670/oceanog.2011.91

Deardorff JW (1980) Stratocumulus-capped mixed layers derived from a three-dimensional model. Boundary Layer Meteorol 18:495–527, doi:10.1007/BF00119502

Deardorff JW (1983) A multi-limit mixed-layer entrainment formulation. J Phys Oceanogr 13:988–1002, doi: 10.1175/1520-0485(1983)013<0988:AMLMLE>2.0.CO;2

Emanuel KA (1999) Thermodynamic control of hurricane intensity. Nature 401:665–669, doi:10.1038/44326

Emanuel KA, DesAutels C, Holloway C, Korty R (2004) Environmental control of tropical cyclone intensity. J Atmos Sci 61:843–858, doi: http://dx.doi.org/10.1175/1520-0469(2004)061<0843:ECOTCI>2.0.CO;2

Jeong YY, Moon I-J, Kim S-H (2013) A study on upper ocean response to typhoon Ewinar (0603) and its impact. Atmos Chem Phys 23:1–16

Joyce RJ, Janowiak JE, Arkin PA, Xie P (2004) CMORPH: a method that produces global precipitation estimates from passive microwave and infrared data at high spatial and temporal resolution. J Hydro 5:487–503

Kawai Y, Wada A (2007) Diurnal sea surface temperature variation and its impact on the atmosphere and ocean: a review. J Oceanogr 63:721–744, doi:10.1007/s10872-007-0063-0

Kepert J, Wang Y (2001) The dynamics of boundary layer jets within the tropical cyclone core. Part II: nonlinear enhancement. J Atmos Sci 58:2485–2501, doi: http://dx.doi.org/10.1175/1520-0469(2001)058<2485:TDOBLJ>2.0.CO;2

Klemp JB, Wilhelmson R (1978) The simulation of three-dimensional convective storm dynamics. J Atmos Sci 35:1070–1096, doi: 10.1175/1520-0469(1978)035<1070:TSOTDC>2.0.CO;2

Kondo J (1975) Air-sea bulk transfer coefficients in diabatic conditions. Bound-Lay Meteorol 9:91–112, doi:10.1007/BF00232256

Lin I-I (2012) Typhoon-induced phytoplankton blooms and primary productivity increase in the western North Pacific subtropical ocean. J Geophys Res 117: C03039, doi:10.1029/2011JC007626

Lin YH, Farley RD, Orville HD (1983) Bulk parameterization of the snow field in a cloud model. J Clim Appl Meteorol 22:1065–1092, doi: 10.1175/1520-0450(1983)022<1065:BPOTSF>2.0.CO;2

Lin I-I, Wu C-C, Emanuel KA, Lee I-H, Wu C-R, Pan I-F (2005) The interaction of supertyphoon Maemi (2003) with a warm ocean eddy. Mon Weather Rev 133:2635–2649, doi:10.1175/MWR3005.1

Lin I-I, Wu C-C, Pun I-F, Ko D-S (2008) Upper-ocean thermal structure and the western North Pacific category 5 typhoons. Part I: ocean features and the category 5 typhoons' intensification. Mon Weather Rev 136:3288–3306, doi:10.1175/2008MWR2277.1

Lin I-I, Pun I-F, Wu C-C (2009) Upper-ocean thermal structure and the western North Pacific category 5 typhoons. Part II: dependence on translation speed. Mon Weather Rev 137:3744–3757, doi:10.1175/2009MWR2713.1

Louis JF, Tiedtke M, Geleyn JF (1982) A short history of the operational PBL-parameterization at ECMWF. In: Proceedings of Workshop on Planetary Boundary Layer Parameterization. ECMWF, Reading., pp 59–79

Moon I-J, Kwon SJ (2012) Impact of upper-ocean thermal structure on the intensity of Korean peninsula landfall typhoons. Prog Oceanogr 105:61–66, doi: http://dx.doi.org/10.1016/j.pocean.2012.04.008

Nam S-H, Kim DJ, Moon WM (2012) Observed impact of mesoscale circulation on oceanic response to Typhoon Man-Yi (2007). Ocean Dyn 62:1–12, doi:10.1007/s10236-011-0490-8

Price JF (1981) Upper ocean response to a hurricane. J Phys Oceanogr 11:153–175, doi: 10.1175/1520-0485(1981)011<0153:UORTAH>2.0.CO;2

Pun IF, Chang Y-T, Lin I-I, Tang TY, Lien R-C (2011) Typhoon-ocean interaction in the western North Pacific: part 2. Oceanography 24:32–41, doi:10.5670/oceanog.2011.92

Qiu B, Chen S (2010) Interannual variability of the North Pacific Subtropical countercurrent and its associated mesoscale eddy field. J Phys Oceanogr 40:213–225, doi:10.1175/2009JPO4285.1

Saito K (2012) The Japan Meteorological Agency nonhydrostatic model and its application to operation and research. In: Yucel I (ed) Atmospheric model applications. InTech, Rijeka, Croatia, pp 85–110. doi:10.5772/35368

Sanford TB, Price JF, Girton JB, Webb DC (2007) Highly resolved observations and simulations of the ocean response to a hurricane. Geophys Res Lett 34: L13604, doi:10.1029/2007GL029679

Sanford TB, Price JF, Girton JB (2011) Upper ocean response to Hurricane Frances (2004) observed by EM-APEX floats. J Phys Oceanogr 41:1041–1056, doi:10.1175/2010JPO4313.1

Shade LR, Emanuel KA (1999) The ocean's effect on the intensity of tropical cyclones: results from a simple coupled atmosphere-ocean model. J Atmos Sci 56:642–651, doi: http://dx.doi.org/10.1175/1520-0469(1999)056<0642:TOSEOT>2.0.CO;2

Shay LK (2010) Air-sea interactions in tropical cyclones. In: Chan JCL, Kepert JD (eds) Global perspective on tropical cyclones from science to mitigation. World Scientific, Singapore, pp 93–132

Shay LK, Mariano AJ, Jacob SD, Ryan ED (1998) Mean and near-inertial ocean current response to hurricane Gilbert. J Phys Oceanogr 28:858–889, doi: http://dx.doi.org/10.1175/1520-0485(1998)028<0858:MANIOC>2.0.CO;2

Soloviev A, Lukas R (2006) The near-surface layer of the ocean: structure, dynamics and application. Atmo Ocean Sci Lib 31:572

Sugi M, Kuma K, Tada K, Tamiya K, Hasegawa N, Iwasaki T, Yamada S, Kitade T (1990) Description and performance of the JMA operational global spectral model (JMA-GSM88). Geophys Mag 43:105–130

Taylor PK, Yelland MJ (2001) The dependence of sea surface roughness on the height and steepness of the waves. J Phys Oceanogr 31:572–590, doi: 10.1175/1520-0485(2001)031<0572:TDOSSR>2.0.CO;2

Usui N, Ishizaki S, Fujii Y, Tsujino H, Yasuda T, Kamachi M (2006) Meteorological Research Institute multivariate ocean variational estimation (MOVE) system: some early results. J Adv Space Res 37:806–822, doi:10.1016/j.asr.2005.09.022

Wada A (2002) The processes of SST cooling by typhoon passage and case study of Typhoon Rex with a mixed layer ocean model. Pap Met Geophys 52:31–66, doi:10.2467/mripapers.52.31

Wada A (2009) Idealized numerical experiments associated with the intensity and rapid intensification of stationary tropical-cyclone-like vortex and its relation to initial sea-surface temperature and vortex-induced sea-surface cooling. J Geophys Res 114:D18111, doi:10.1029/2009JD011993

Wada A (2012) Oceanic influences for a large eye of Typhoon Talas in 2011. CAS/JSC WGNE Res Activ Atmos Oceanic Model 42:9.09–9.10

Wada A, Usui N (2007) Importance of tropical cyclone heat potential for tropical cyclone intensity and intensification in the Western North Pacific. J Oceanogr 63:427–447, doi:10.1007/s10872-007-0039-0

Wada A, Niino H, Nakano H (2009a) Roles of vertical turbulent mixing in the ocean response to Typhoon Rex (1998). J Oceanogr 65:373–396, doi:10.1007/s10872-009-0034-8

Wada A, Usui N, Sato K, Kawai Y (2009b) Comment on "Importance of pre-existing oceanic conditions to upper ocean response induced by Super Typhoon Hai-Tang" by Z.-W. Zheng, C.-R. Ho and N.-J. Kuo. Geophys Res Lett 36:L09603

Wada A, Kohno N, Kawai Y (2010) Impact of wave-ocean interaction on Typhoon Hai-Tang in 2005. SOLA 6A:13–16, doi:10.2151/sola.6A-004

Wada A, Cronin MF, Sutton AJ, Kawai Y, Ishii M (2013) Numerical simulations of oceanic pCO_2 variations and interactions between Typhoon Choiwan (0914) and the ocean. J Geophys Res 118:1–18, doi:10.1002/jgrc.20203.2013

Walker ND, Leben RR, Balasubramanian S (2005) Hurricane-forced upwelling and chlorophyll a enhancement within cold-core cyclones in the Gulf of Mexico. Geophys Res Lett 32:L18610, doi:10.1029/2005GL023716

Warner JC, Armstrong B, He R, Zambon JB (2010) Development of a coupled ocean-atmosphere-wave-sediment transport (COAWST) modeling system. Ocean Model 35:230–244, doi:10.1016/j.ocemod.2010.07.10

Wu L, Wang B, Braun SA (2005) Impacts of air-sea interaction on tropical cyclone track and intensity. Mon Weather Rev 133:3299–3313, doi: http://dx.doi.org/10.1175/MWR3030.1

Wu C-C, Lee CY, Lin I-I (2007) The effect of the ocean eddy on tropical cyclone intensity. J Atmos Sci 64:3562–3578, doi:10.1175/JAS4051.1

Zhu H, Ulrich W, Smith RK (2004) Ocean effects on tropical cyclone intensification and inner-core asymmetries. J Atmos Sci 61(Zhu H, Ulrich W, Smith RK): 1245–1257, doi: http://dx.doi.org/10.1175/1520-0469(2004)061<1245:OEOTCI>2.0.CO;2

doi:10.1186/2197-4284-1-11
Cite this article as: Wada *et al.*: Typhoon-induced sea surface cooling during the 2011 and 2012 typhoon seasons: observational evidence and numerical investigations of the sea surface cooling effect using typhoon simulations. *Progress in Earth and Planetary Science* 2014 **1**:11.